THE JOURNAL OF PHYSICAL CHEMISTRY B

Article

pubs.acs.org/JPCB

Viscoelastic Behavior and Reinforcement Mechanism in Rubber Nanocomposites in the Vicinity of Spherical Nanoparticles

P. Bindu*[,†,‡] and Sabu Thomas[†,‡]

[†]School of Chemical Sciences, Mahatma Gandhi University, Priyadarshini Hills P.O, Kottayam, Kerala, India 686 560

[‡]Centre for Nanoscience and Nanotechnology, Mahatma Gandhi University, Kottayam, Kerala, India 686 560

Supporting Information

ABSTRACT: The viscoelastic behavior and reinforcement mechanism of nano ZnO reinforced natural rubber (NR) nanocomposites were investigated in this study. Dynamic mechanical analysis was performed to investigate the nature of the constrained polymer region in NR−nano ZnO nanocomposites, and the constrained polymer region is responsible for the reinforcement mechanism. The viscoelastic and tensile properties of NR nanocomposites were investigated with respect to the effect of nanofiller loading. All the nanocomposites showed a significant increase in storage modulus in the glassy and rubbery regions, the shift of the tan δ peak to the higher temperature region, and the lowering of the tan δ peak intensity compared to neat NR. The enhancement in the modulus is related to the weight % of the added nano ZnO as well as the volume of the constrained rubber chains in the proximity of ZnO nanoparticles. The study of the constrained volume of the polymer indicates that the structure of the nanocomposite possesses a moderately strong interfacial interaction between rubber chains and ZnO nanoparticles. The type of rubber−nanofiller interaction strongly influences the amount and modulus of the constrained region and contributes to the enhancement in the storage modulus of the resulting nanocomposites. The volume fraction of the constrained region of the NR nanocomposites was found to have good linear correlation with the weight % of nano ZnO. It was also understood that there should exist an optimum cross-linking density for a certain nanofiller reinforced rubber system, as well as partial physical adsorption of macromolecular rubber chains on the nanofiller surface. An optimum nanofiller loading is necessary for moderately strong rubber−nanofiller interaction and hence for the enhancement in the mechanical properties of the NR nanocomposites. A core−shell morphology model and constrained polymer model have been proposed to explain the constrained polymer chains in the NR−nano ZnO nanocomposite system on the basis of these results.

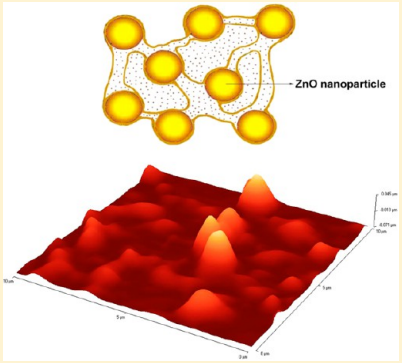

1. INTRODUCTION

The reinforcement of polymers using nanofillers is commonly undertaken in the production of high-performance polymer nanocomposites. The uniform dispersion of nanoparticles can lead to a very large interfacial area in which the distance between the nanoparticles begins to approach molecular dimensions. The interactions between the organic and inorganic phases create polymer nanocomposites with possible synergistic properties.

Natural rubber (NR) is a polymer of isoprene units linked together at 1−4 positions and arranged in the cis configuration. This is one of the most fascinating and important industrial polymers among many engineering polymers.[1] NR has high green strength due to the presence of nonrubber components, such as phospholipids and proteins,[2] and its ability to crystallize upon stretching in unvulcanized and vulcanized states,[3] which is determined from the nonrubber components and the high stereoregularity[4] of NR. In common practice, enhancement of the mechanical properties of NR is achieved by the introduction of chemical cross-links as well as the addition of finely divided particulates, typically carbon black, silica, or clay. A minimum of 20−30 wt % of conventional filler is required to attain optimal mechanical properties, but this high concentration reduces the processability and increases the weight of the final product. The continuous demand for new, low-cost, low-weight rubber composites with improved properties represents a challenge in the rubber industry. Rubber nanocomposites have attracted many researchers due to their unique properties. As compared with microfiller-reinforced rubber, nanofiller-reinforced rubber exhibits high hardness, modulus, antiaging, and gas barrier properties. Therefore, the nano concept is highly relevant for rubber compounds since their applications require filler reinforcement. The great improvement in properties associated with the addition of small fractions of nanofiller in a polymer matrix has aroused a relevant amount of research in the academic and industrial communities.[5] The polymer chains in the proximity of nanofillers are constrained because of their interactions with the well-dispersed nanofillers, and these constrained polymer chains are responsible for the enhancement of the properties of

Received: April 21, 2013
Revised: August 12, 2013
Published: October 3, 2013

NR nanocomposites. Recently, Adame and Beall[6] used atomic force microscopy (AFM) to measure the constrained region in amorphous polyamide/nanoclay nanocomposites. It was found that the constrained polymer region is approximately a spheroid in shape and that the region exhibits a much lower diffusion coefficient than the bulk polymer.

The clear understanding of the reinforcing mechanism of nanocomposites is important in the design of nanomaterials with desirable properties. The reinforcing effect of carbon black is primarily due to hydrodynamic interactions between the rubber and filler surfaces.[7] Sternstein et al.[8] have found experimentally that the mechanism for reinforcement in nanocomposites is attributed to filler−matrix interactions, rather than filler agglomeration or percolation. It was reported that, in NR−nano TiO_2 nanocomposites[9] and NR−organoclay nanocomposites,[10] there exists a strong interfacial interaction between the rubber matrix and the nanofiller. In NR−pretreated CNT nanocomposites,[11] the strong interfacial bonding between the CNTs and the rubber molecules were observed, and therefore, the CNTs can transfer stress effectively throughout the rubber matrix and play an important role in the reinforcement in NR nanocomposites. López-Manchado et al.[12] have discussed that, in nanoclay−NR-vulcanized nanocomposites, the presence of nanoclay introduces a dual crystallization mechanism due to the alignment of clay nanoparticles during stretching. The improved properties of NR−nanoclay nanocomposites can be attributed to microstructural and morphological changes induced by nanoclay in the NR matrix during crystallization. All of these factors during deformation contribute to the formation of a network structure containing cross-linked chemical chains, nanofiller, and crystallizable networks in the NR−nanoclay nanocomposite. Dishovsky et al.[13] have reported that carbon black filled NR-containing graphine nanoparticles (GNPs) were found to improve the dielectric properties and microwave properties, viz., coefficients of absorption and reflection of the electromagnetic waves and electromagnetic interference shielding effectiveness. Stiffness improvement by thermally reduced graphine oxide (TRG) was found to be more pronounced for elastomers,[14] such as NR, styrene butadiene rubber (SBR), and thermoplastic polyurethane (TPU), than glassy polymers,[15] such as polycarbonate (PC) and poly(ethylene-2,6-naphthalate (PEN), due to the higher stiffness contrast between the matrix and the nanofiller. Of late, we have estimated the volume fraction of the constrained region in prevulcanized NR latex−nano ZnO nanocomposites,[16] and our studies support the existence of moderately strong rubber−nano ZnO interaction in prevulcanized NR latex nanocomposites, because of the strong electrostatic adhesion between the counterions and the ionic surfactant at the interface between polymer charged particles. Recent reports from our lab show that cellulose nanofibers[17] and cellulose nanowhiskers[18] are expected to form an entangled network in the cross-linked NR phase, thereby restricting the mobility of rubber chains and improving the mechanical properties of the resulting nanocomposites.

Zinc oxide (ZnO) is one of the basic components of rubber compounds. In the vulcanization of natural rubber (NR), conventional ZnO (micro) is used as an activator, and in general practice, about 5 phr (parts by weight per 100 g of rubber) is the dosage. The reduction in the quantity of ZnO is worthwhile because it has high density and some soluble zinc compounds have been classified as toxic to aquatic species. In the past years, a totally different and new approach to reduce ZnO in rubber compounding was introduced by Hepburn et al.,[19] the use of multifunctional additives (MFAs), such as a bifunctional diamine, which can function as a simultaneous cure activator and accelerator for sulfur vulcanization, and it was found that the use of ZnO and stearic acid in the compound formulation was not necessary. In previous years, most of the relevant research[20] about nano ZnO was focused on using it as a substitute for micro ZnO in the sulfur vulcanization of rubber compounds. Of late, considering this problem, the use of nano ZnO in natural rubber[21] and neoprene rubber was studied.[22] Moreover, the Environmental Protection Agency (EPA) and the European Union have classified ZnO as a hazardous chemical for the aquatic environment and proclaimed that its application in rubber technology should be reduced and controlled[23] in order to alleviate the difficulty in disposing of waste rubber compounds. Considering this ecological point of view, it is advisable to keep the ZnO content as low as possible in making the rubber products with ZnO.

Therefore, the present study emphasizes the use of nano ZnO as cure activator and reinforcing agent in NR instead of conventional micro ZnO. The central theme of the present study is to investigate the viscoelastic behavior and reinforcement mechanisms in nano ZnO/NR nanocomposites using theoretical modeling. We expect that the present study is an important contribution, and very scant information was reported[21] in the literature regarding the use of nano ZnO as a cure activator in the sulfur vulcanization of natural rubber. The morphology of NR composites containing nano ZnO was analyzed by transmission electron microscopy (TEM), scanning electron microscopy (SEM), and atomic force microscopy (AFM). The mechanical properties, gas permeability, free volume measurements by positron annihilation lifetime spectroscopy (PALS), determination of cross-link density, and calculation of diffusion coefficient of composites containing nano ZnO have been carried out and presented in this paper. The studies revealed that moderately strong rubber−filler interactions exist in NR nanocomposites.

2. EXPERIMENTAL SECTION

Materials. The natural rubber (NR), ISNR-5 of Mooney viscosity ML (1 + 4) at 100 °C equal to 85, was obtained from the Rubber Research Institute, Kottayam, Kerala, India. The molecular weight of NR obtained by light scattering is M_n = 2.68 × 10^5 g/mol, M_w = 8.38 × 10^5 g/mol, and M_w/M_n = 3.1. Sulfur and stearic acid were obtained from Merk, Mumbai, India, and accelerators, viz., *N*-cyclohexylbenzothiazole-2-sulphenamide (CBS) and tetramethylthiuram disulfide (TMTD) were supplied by NOCIL Ltd. Mumbai, India. The chitosan sample was provided by M/s India Sea Foods, Cochin, Kerala, India. Zinc chloride and sodium hydroxide were supplied by M/s. SD. Fine Chem Ltd. Mumbai, India. Nano ZnO was synthesized from chitosan, zinc chloride, and sodium hydroxide.

Preparation of ZnO Nanoparticles. ZnO nanoparticles were synthesized from $ZnCl_2$ and chitosan by a precipitation method.[16]

Preparation of NR Composites Containing Nano ZnO. Natural rubber (NR) (100 g) was masticated in a two-roll mill; after that, 0.5 g of nano ZnO and 2.5 g of coactivator stearic acid were added and again masticated. Milling was continued by the successive addition of the accelerators CBS (0.6 g) and TMTD (0.1 g), and the vulcanizing agent sulfur (2.5 g). The NR composites with varying weight percentages of nano ZnO,

dx.doi.org/10.1021/jp4039489 | J. Phys. Chem. B 2013, 117, 12632−12648

viz., 1, 2, and 3 g, were also prepared in the same manner. Table 1 shows the formulations[21] used for preparation.

Table 1. Formulation[a] and Compound Designation for NR Nanocomposites

	compound designation			
formulation	NR-N0.5	NR-N1	NR-N2	NR-N3
NR	100	100	100	100
nano ZnO	0.5	1.0	2.0	3.0
stearic acid	2.5	2.5	2.5	2.5
CBS	0.6	0.6	0.6	0.6
TMTD	0.1	0.1	0.1	0.1
sulfur	2.5	2.5	2.5	2.5

[a]All weights are in parts per 100 g of rubber (phr). CBS, *N*-cyclohexylbenzothiazole-2-sulphenamide; TMTD, tetramethyl thiuram disulfide.

Characterization Methods. ZnO nanoparticles were characterized by FTIR (Schimadzu IR-470 IR spectrophotometer) (KBr pellet, in the range 4000−400 cm^{-1}), XRD (Xpertpro-Panalytical machine, λ = 1.54060 Å, Cu−Kα), SEM (FE-SEM SUPRA-25 ZEISS analyzer), and HRTEM (JEOL-JEM 3010 instrument, under an accelerating voltage of 200 kV) as reported.[16]

The SEM images of the rubber nanocomposites were taken with the help of a JEOL 840 analyzer with a W-filament, secondary E-T, and a solid-state backscattered electron detector. The Be-window EDS system (EDAX) (Oxford Instruments) with a resolution at 20 kV, 10 nm was used. HRTEM is the most effective method for the analysis of dispersion of nanoparticles in polymer nanocomposites. The nanocomposite samples for TEM analysis were prepared by ultracryomicrotomy with a Leica Ultracut UCT (Leica Microsystems GmbH, Vienna, Austria). Freshly sharpened glass knives with cutting edges of 45° were used to obtain cryosections of about 100−150 nm in thickness at −110 °C. The cryosections were collected individually in sucrose solution and directly supported on a copper grid of 300 mesh. Microscopy was performed with a JEOL 2100, Japan. The transmission electron microscope was operated at an accelerating voltage of 200 kV. The surface morphology of rubber nanocomposites was obtained by AFM. AFM images were obtained by using a Veeco di Innova AFM microscope. The rubber samples were kept in phase contrast tapping mode with a frequency of 258 kHz and a scan rate of 1 Hz. The AFM measurements were carried out in air at ambient conditions (25 °C).

Cure characteristics of NR−nano ZnO nanocomposites were done using a MDR-2000 rheometer at 150 °C. The samples were cured at their respective cure times using a hydraulic press under a pressure of about 120 bar at 150 °C. The cured samples were used for further analysis. The density of the nanocomposites was measured using an M-200S electronic densimeter.

For the measurement of water resistance and calculation of diffusion coefficient, circular samples of 2 cm in diameter were cut from polymer sheets by means of a standard die. The thickness and initial weight of the samples were noted. Distilled water was allowed to diffuse through the samples at room temperature, and the weight of the nanocomposite samples was checked every hour. The measure of water uptake at two different parameters was plotted, viz., time and weight % of nano ZnO. Water diffusion coefficients were also measured from the slope of these graphs. Cross-link density values of the samples were determined by an equilibrium swelling method using toluene as the solvent. Circular samples were punched from the sheet, the weighed samples were kept in toluene until they reached equilibrium swelling, and then the weights were taken for the calculation.

The positron lifetime spectrometer, consisting of a fast−fast coincidence system with BaF_2 scintillators coupled to photomultiplier tubes of type XP2020/Q with a quartz window as detectors in a conical shape to achieve better time resolution, was used for the free volume measurements. A 17 μCi ^{22}Na positron source, deposited on a pure Kapton foil of 0.0127 mm in thickness, was placed between the two identical pieces of the sample under investigation, and this was placed between the two detectors of PALS to acquire the lifetime spectrum. The spectrometer was operated at a 180 ps time resolution with ^{60}Co as the source; however, for a better count rate, the spectrometer was operated at a 220 ps time resolution. All lifetime measurements were performed at room temperature. In the PALS analysis of polymers, only two measured parameters, viz., *ortho*-positronium (*o*-Ps) lifetime (τ_3) and *o*-Ps intensity I_3, are important since they provide free volume information. The *o*-Ps lifetime (τ_3) measures the size of the free volume holes (V_f), and I_3 is a relative measure of the number of free volume sites in the polymer matrix. The free volume cavity radius (R) is related to the *o*-Ps pick-off lifetime (τ_3) by a simple relation. The free volume is assumed as a spherical potential well-surrounded by an electron layer of thickness ΔR, and the size of the free volume holes can be calculated using the following semiempirical equation[24]

$$\tau_3 = \frac{1}{2}\left[1 - \left(\frac{R}{R_0}\right) + \left(\frac{1}{2\pi}\right)\sin\left(\frac{2\pi R}{R_0}\right)\right]^{-1} \quad (1)$$

where τ_3 (*ortho*-positronium (*o*-Ps) lifetime) and R (radius of free volume holes) are expressed in nanoseconds and nanometers, respectively. $R_0 = R + \Delta R$, where ΔR (ΔR = 0.166 nm) represents the thickness of the electron layer or the probability of overlap of the Ps wave function with the electron wave function.[25] Using this value of R, the free volume size (V_f) was calculated as $V_f = (4/3)\pi R^3$. The fractional free volume was then evaluated as the product of free volume (V_f) and *o*-Ps intensity I_3 (%); that is, $F_v = CV_fI_3$, where the constant C is 0.0018 $Å^{-3}$.[25]

The air permeability of the NR−nano ZnO composite membranes was measured using a Lyssy Manometric gas permeability tester L100−2402. Oxygen was used as the test gas, at a rate of 500 mL/min. The circular-shaped samples having a diameter of 10 cm and a thickness of 1 mm were used. Permeability of the samples was calculated using the equation, $P_m = (T_r \times P_r)/t_m$, where P_m is the permeability of the test sample, t_m is the interval time constant for the test sample, P_r is the permeability of the reference (standard PET sample), and T_r is the interval time constant for standard PET. The test was conducted at a temperature of (25 ± 1)°C and a relative humidity of 65 ± 0.5.

The tensile strength, tensile modulus, and elongation at break were measured by the ASTM method with a Zwick 1474 Universal testing machine using dumbbell-shaped samples.

dx.doi.org/10.1021/jp4039489 | J. Phys. Chem. B 2013, 117, 12632−12648

3. RESULTS AND DISCUSSION

The ZnO nanoparticles were synthesized from $ZnCl_2$ and chitosan and characterized by FT-IR, XRD, SEM, and TEM.[16]

The theoretical density of the composites was calculated using the equation

$$\rho_c = \rho_p(1 - V_1) + \rho_f V_1 \quad (2)$$

where ρ_c is the density of the composite, ρ_p is the density of the polymer, ρ_f is the density of the filler, and V_1 is the volume fraction of the filler. Using the theoretical and experimental densities, the porosities of the composites were also calculated by using the equation

$$\text{Porosity}\,(\%) = (\text{difference in density/true density}) \times 100$$

The density (experimental) of the nanocomposites does not show much increase with the increase in nano ZnO content, as only small amounts of nano ZnO were added. For NR nanocomposites, the density shows a slight increase up to 2 phr of nano ZnO and decreases after further addition of nano ZnO. The experimental and theoretical density were compared, and the porosity of the composites was calculated. The density of all the rubber nanocomposites is given in Table 2. The porosity of

Table 2. Density, Porosity, and Diffusion Coefficient (D)[a]

sample	experimental density (kg/m^3)	theoretical density (kg/m^3)	porosity (%)	diffusion coefficient (D) ($\times 10^{-2}$ cm^2 s^{-1})
NR-N0.5	0.8992	0.9120	1.40	1.30
NR-N1	0.9015	0.9139	1.36	1.07
NR-N2	0.9075	0.9183	1.18	0.96
NR-N3	0.9135	0.9268	1.44	1.59

[a]Neat NR D: 1.95 $\times$ 10^{-2} cm^2 s^{-1}.

NR−nano ZnO nanocomposites decreases from 0.5 to 2 phr with the addition of nano ZnO and increases with further addition of nano ZnO, which is due to the aggregation of ZnO nanoparticles. The lowest porosity (1.18%) was observed for the composite with 2 phr of nano ZnO (i.e., NR-N2).

The diffusion of water is strongly influenced by the microstructure of the nanocomposites. Water absorption of NR nanocomposites is plotted as a function of time in Figure 1. When the nano ZnO content was less than 2 phr, water absorption was higher. In this case, water uptake is minimum for NR-N2 nanocomposite and the percent of water uptake decreases with the increase in nano ZnO content up to a particular phr, *viz.*, 2 phr, for NR-N2. Since water absorption of nanocomposites is influenced by porosity, the nanocomposite with less porosity, that is, NR-N2, exhibits a very low percent of water uptake

$$\text{Water uptake}\,(\%) = \frac{(W_t - W_0)}{W_w} \times 100 \quad (3)$$

where W_t is the weight of sample at time (1 h, 2 h...), W_0 is the weight of the sample at zero time, and W_w is the weight of the sample at infinite time.

The water diffusion coefficient (D) of the nanocomposites can be calculated as[26]

$$D = \pi\left(\frac{h\theta}{4M_w}\right)^2 \quad (4)$$

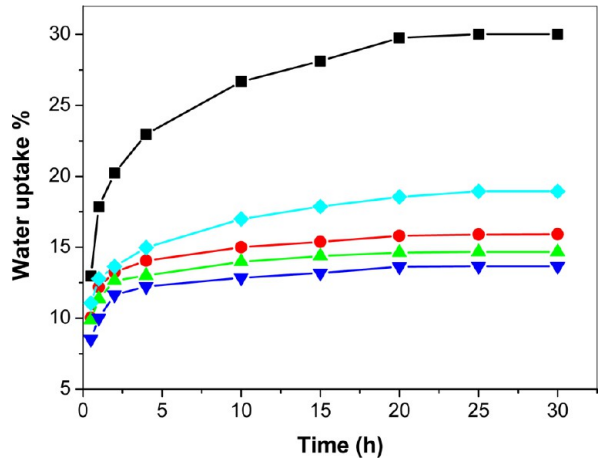

Figure 1. Effect of time on the % of water uptake of NR nanocomposites: (black square) neat NR, (red circle) NR-N0.5, (green triangle) NR-N1, (blue triangle) NR-N2, (aqua diamond) NR-N3.

where D is the water diffusion coefficient, h is the thickness of each sample, θ is the slope of the linear portion of the curve, and M_w is the weight of each sample at infinity. The water diffusion coefficients of the nanocomposites were evaluated and are summarized in Table 2. The value is minimum for the NR-N2 nanocomposite. When ZnO nanoparticles were introduced into the rubber matrix, they occupy the pores or free volume voids within the matrix. The percent of water absorption of nanocomposites depends on the porosity of the nanocomposites. The percent of water absorption and porosity decreases from 0.5 to 2 phr with the addition of nano ZnO. Among the nanocomposites, NR-N2 exhibited the lowest value of porosity and diffusion coefficient; this emphasizes that the segmental motion of the rubber chains are considerably restricted due to the increase in the weight % of nano ZnO. It can also result from a strong interaction between the nanofiller and the matrix, which limits the diffusion of water within the entangled polymer matrix. As the weight % of nano ZnO increases from 0.5 to 2 phr, the volume of the entangled polymer matrix increases due to the high amount of nanofiller−matrix interaction. Further addition of nano ZnO (i.e., 3 phr) brings more nanoparticle−nanoparticle interaction rather than nanoparticle−matrix interaction, which produces aggregation of ZnO nanoparticles in the matrix; and therefore, the number of independent nanoparticles decreases and surface area also decreases. The porosity and diffusion coefficient values are the highest for NR-N3, because the aggregated nanoparticles can not effectively restrict the segmental motion of rubber chains due to the poor nano ZnO−rubber matrix interaction. This is the reason for the increased porosity and diffusion coefficient values of NR-N3. However, the smaller value of porosity and diffusion coefficient indicates moderately strong rubber−filler interactions at this composition.

The cross-link density can be calculated from the swelling method using the equation,[27] and the variation of cross-link density with weight % of nano ZnO is shown in Figure 2

$$\nu = \frac{1}{2M_c} \quad (5)$$

where M_c is the molar mass between cross-links of dynamically vulcanized samples. M_c is calculated by equilibrium swelling in toluene using the Flory−Rehner equation[28]

dx.doi.org/10.1021/jp4039489 | J. Phys. Chem. B 2013, 117, 12632−12648

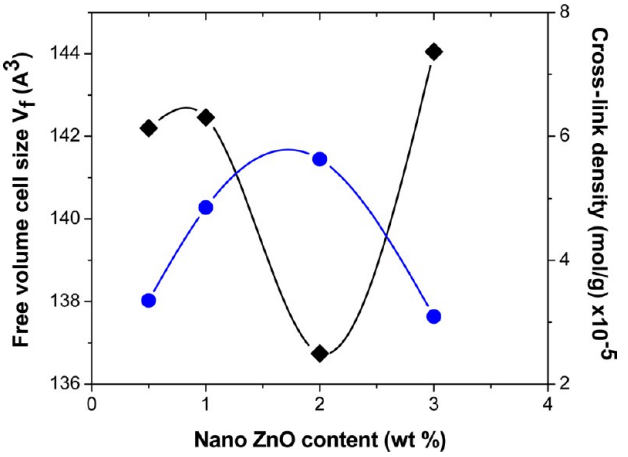

Figure 2. Variation of cross-link density and free volume cell size with weight % of nano ZnO: (black diamond) free volume cell size, (blue circle) cross-link density.

$$M_c = \frac{-\rho_p V_s V_r^{1/3}}{\ln(1 - V_r) + V_r + \chi V_r^2} \quad (6)$$

where ρ_p is the density of the polymer, V_s is the molar volume of the solvent, χ is the rubber solvent interaction parameter, and V_r is the volume fraction of swollen rubber, which is given by the Ellis and Welding equation[29]

$$V_r = \frac{(d - f_1 w)\rho_p^{-1}}{(d - f_1 w)\rho_p^{-1} + A_s \rho_s^{-1}} \quad (7)$$

where d is the deswollen weight of the sample, f_1 is the volume fraction of the insoluble component, w is the initial weight of the sample, ρ_s is the density of the sample, and A_s is the amount of the solvent absorbed. The interaction parameter is given by[30]

$$\chi = \beta + \frac{V_s}{RT}(\delta_s - \delta_p)^2 \quad (8)$$

where V_s is the molar volume of the solvent, δ_s and δ_p are the solubility parameters of the solvent and polymer, respectively, R is the universal gas constant, T is the absolute temperature, and β is the lattice constant.

The variation of cross-linking density determined from the swelling measurements by changing the weight % of nano ZnO comes from the contribution from the immobilized polymer chains constrained by the nanofiller surface. This argument could be supported by the rate of vulcanization we have obtained from the rheometer studies (provided in the Supporting Information). The rate of vulcanization is maximum at low nano ZnO content (0.5 phr), as evidenced by the highest value of cure rate index for this formulation. This means that the cross-linking efficiency of the ZnO as an accelerator activator is maximum at low concentration of nano ZnO. Therefore, the observed changes in cross-link density comes from the constrained polymer layers on the nano ZnO filler surface and not due to the extra cross-links formed by the cure activation process by the increasing concentration of nano ZnO. From the rheometer studies, it can be seen that there is absolutely no cure activation beyond 0.5 phr of nano ZnO. As the weight % of nano ZnO increases from 0.5 to 2 phr in the NR matrix, more rubber chains are constrained or immobilized due to the reinforcing action of nano ZnO. Thus, due to the presence of more constrained rubber chains in the NR nanocomposites, the position of the glass transition temperature T_g is shifted to a higher temperature region than that of the neat NR. In particular, viscoelastic response is very much sensitive to the extent of rubber−nanofiller interaction of the system.

Thermodynamic effects occurring during swelling of the elastomer chains were also analyzed. The thermodynamic approach is of great importance for understanding the rubber−filler interaction in the nanocomposites. Swelling of a sample depends on the cross-link density and the solvent used. The swelling of the rubber in the presence of a solvent will significantly modify the conformational entropy (ΔS) and the elastic Gibbs free energy (ΔG). The elastic Gibbs free energy can be determined from the Flory−Huggins equation.[31]

$$\Delta G = RT[\ln(1 - V_r) + V_r + \chi V_r^2] \quad (9)$$

From the statistical theory of rubber elasticity, ΔS can be obtained from the equation $\Delta G = -T\Delta S$, which indicates that no change in internal energy of the network occurs upon stretching. Both thermodynamic parameters, ΔS and ΔG, of the composites are reported in Table 3. It should be noted that

Table 3. Thermodynamic Parameters ΔG and ΔS of Swelling (in Toluene)

sample	ΔG (J/mol)	ΔS (J/mol) × 10^{-2}
NR-N0.5	−8.69	2.83
NR-N1	−13.35	4.35
NR-N2	−15.68	5.11
NR-N3	−8.17	2.66

addition of nano ZnO up to 2 phr increases the ΔG value, after that, it decreases. It is assumed that ΔG is closely related to the elastic behavior of the material; that is, the nanocomposites show better elasticity than the microcomposite. These results can be attributed to better compatibility between nano ZnO and rubber. The addition of higher amount of nano ZnO (i.e., 3 phr) causes aggregation of nanoparticles in the rubber matrix, and the uniform dispersion of nano ZnO becomes impossible.

The NR-N2 nanocomposite showed a slightly higher cross-link density compared with NR-N0.5 and NR-N1 nanocomposites. During the swelling experiment, the amount of solvent absorbed by the sample decreases, and hence, the value of volume fraction of the polymer in the solvent-swollen condition increases, leading to higher cross-link density. The small increase in cross-link density of rubber nanocomposites with the addition of 2 phr of nano ZnO shows the reinforcement of rubber and nano ZnO (Figure 2). The higher cross-link density values indicate more strain on the network due to restricted chain mobility and thus results in lower swelling due to the presence of nanofiller. When the number of cross-links per unit volume increases, the transport of gas molecules through the highly cross-linked rubber membrane becomes very difficult. This is supported from free volume data described in the following section.

Positron Annihilation Lifetime Spectroscopy (PALS). Free volume is a frequently used microstructure parameter that can reflect the motion of polymer-chain segments and thus plays an important role in deciding the mechanical properties, diffusion of small molecules through a polymer, and so on.[32,33] PALS is based on the fact that the positronium (Ps) atoms formed in polymers are predominantly localized in the atomic

dx.doi.org/10.1021/jp4039489 | J. Phys. Chem. B 2013, 117, 12632−12648

scale and nanoscale holes[33] and is becoming an increasingly important method to detect nanoscale holes in polymers. The purpose of the present research is to investigate the effects of nanodispersed ZnO on the free volume characteristic of natural rubber−ZnO nanocomposites. The molecular and free volume theories help to describe the diffusion of permeant through polymeric membranes. According to free volume theory, the diffusion is not a thermally activated process as in a molecular model. It is assumed to be the result of random redistributions of free volume voids within a polymer matrix, and free volume provides the pathways for the permeant.

The effect of nano ZnO on *o*-Ps lifetime (τ_3), *o*-Ps intensity (I_3 (%)), and the fractional free volume (%) of rubber nanocomposites are presented in Table 4. It can be seen from

Table 4. PALS Measurement Data

sample	*o*-Ps lifetime τ_3 (ns) ± 0.02	*o*-Ps intensity I_3 (%) ± 0.13	fractional free volume F_v (%)
NR-N0.5	2.45	14.17	3.63
NR-N1	2.45	13.67	3.50
NR-N2	2.39	13.55	3.33
NR-N3	2.50	17.30	4.48

the table that the free volume cell size and fractional free volume are the lowest for the NR-N2 nanocomposite. It is also clear that the free volume cell size (Figure 2) and fractional free volume (Table 4) decrease up to 2 phr of nano ZnO in the NR nanocomposites and increased upon higher loading of nano ZnO (i.e., 3 phr), which is attributed to the existence of a higher amount of nanoparticle−nanoparticle interaction than the rubber−nanoparticle interaction, leading to aggregation of nanoparticles in the rubber matrix and the consequent additional void formation. In the rubber matrix, highly structured filler aggregates typically have branches, which can form voids between them, where polymer can be occluded. Nonspherical filler particle aggregates have a volume packing less dense than that of spherical particles, leaving a greater volume of voids between the particles. The reason for the decrease in free volume cell size in rubber nanocomposites was the restricted mobility of the chain segments in the presence of nano ZnO, which established more cross-links and also reduces permeation by virtue of increasing the diffusion path length. In the present study, we would like to underline the fact that nano ZnO has a dual function; it has the ability to act as the cure activator for rubber vulcanization (cross-linking) and, at the same time, can act as an excellent filler for the reinforcement of rubber. The reaction of nano ZnO with stearic acid, accelerators, sulfur, and rubber can be explained as follows. As the surface-to-volume ratio of nano ZnO is much larger than that of micro ZnO, its reaction with stearic acid and accelerators is very fast and accelerates the formation of the zinc−accelerator complex. This complex is more reactive than the free accelerator and helps sulfur insertion to occur more rapidly in the rubber molecules. The Zn−accelerator complex interacts with sulfur or sulfur donors to form the very active sulfurating agent, which reacts with allylic sites of rubber chains to form an increased number of cross-link precursors. The cross-link precursors react with another elastomer chain to produce an increased number of cross-links. It can be argued that the high surface area of nano ZnO accelerates the adsorption of accelerators, sulfur, and stearic acid on its surface and hence can act both as a reactant and as a catalytic reaction template. The role of nano ZnO as a reinforcing agent is due to the physical adsorption of the rubbery chains at the surface of the nano ZnO particles, leading to immobilized macromolecular chains around the nanoparticles. Our obervations are in agreement with the exciting work of Montes et al.[34] on ^{1}H NMR experiments on filled rubbers, which allowed the observation of two features: the introduction of supplementary topological constraints by the fillers, and a layer of immobilized segments at the particle surface. The contact surface area between the filler and the matrix is higher in nanocomposites due to the high aspect ratio of nanofiller, which, in turn, reduces the free volume concentration (F_v). Wang et al.[35] and Stephen et al.[28] studied the impact of nanoparticles on the free volume and the barrier properties and arrived at the conclusion that the permeability of a nanocomposite was mainly due to the influence of fractional free volume.

Gas Permeability. Free volume cells or "holes" exist in the rubber matrix. The "holes" thermally form and disappear with the movement of polymer chains. Gases are soluble in rubber-like substances. When rubber is exposed to a gas, solution occurs at the surface and the dissolved gas molecules diffuse into the interior. The diffusion of gas molecules in the rubber membrane is a process in which the gas molecules migrate from "holes" (free volume) to "holes" (free volume). The permeation of gas through a membrane involves solution on one side, then diffusion through the membrane to the other side, and finally evaporation out of the membrane.[36] Since the rate of permeation is a specific function of a given gas and rubber, the rate of permeation depends on both solubility and the rate of diffusion. The polymeric membranes used for gas separation processes have certain significance, such as high permeability to the desired gas, high selectivity, and the ability to form useful membrane configurations.

The oxygen permeability of the nano ZnO filled composites having a thickness of 1 mm were tested and compared with that of reported micro ZnO filled NR composites.[37] We found that the permeability was significantly decreased as the nano ZnO content was increased, reaching a minimum for a composition of 2 phr of nano ZnO. The permeability of the NR-N2 nanocomposite was found to be decreased by 17% as that of the micro ZnO fillled NR composite. Addition of nano ZnO can considerably improve the gas barrier property of NR, even at relatively low loading. It was found that the transport of oxygen gas through the nano ZnO filled membrane was lower than that of the micro ZnO filled one.[37] The enhancement in gas barrier properties of the nano ZnO reinforced membrane indicates the existence of moderately strong rubber−nanofiller interaction and reduced availability of free volume, and as a result, the permeability of the filled membrane decreases. The enhanced gas barrier property of the nano filled membrane is due to the homogeneous dispersion and high aspect ratio of the nanofiller than that of the microfiller. Because of the high aspect ratio of the nanofiller, the contact area between the filler and the matrix increases. The reinforcement of nano ZnO in the rubber matrix was supported by porosity, diffusion coefficient, and cross-link density values. The low values of fractional free volume (Table 4) and higher cross-link density values are responsible for the improved selectivity of nanocomposite membranes.

Morphology Characterization. The phase morphology of nanocomposites was taken. Figure 3a,b shows the SEM micrograph and EDAX of NR-N2. From the SEM image, it was clear that the nano ZnO was embedded within the NR

dx.doi.org/10.1021/jp4039489 | J. Phys. Chem. B 2013, 117, 12632−12648

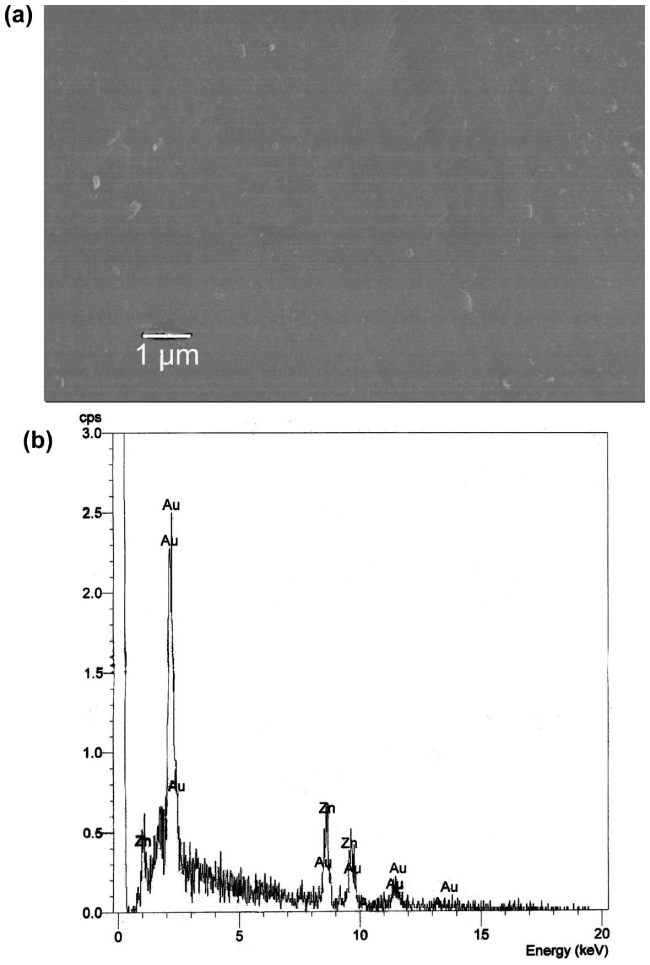

Figure 3. (a) SEM image of NR-N2. (b) EDAX of NR-N2.

matrix. The ZnO nanoparticles appear as small white grains or dots and are homogeneously dispersed in the NR matrix. The EDAX confirms the presence of nano ZnO embedded in the rubber matrix. The samples were coated with a film of Au before irradiation of an electron beam, hence the presence of the Au peak in the EDAX.

The TEM analysis was carried out to get an idea regarding the dispersion of ZnO nanoparticles in the matrix. The transmission electron micrographs (TEM) of rubber nanocomposites are presented in Figure 4a,b. The small dark spots in the transmission electron micrographs show the dispersion of nano ZnO in the rubber matrix. When the nano ZnO content varies from 0.5 to 2 phr, ZnO nanoparticles are homogeneously dispersed in the matrix. Figure 4a shows the homogeneous dispersion of ZnO nanoparticles in NR-N2. However, it can be seen from Figure 4b that, as the concentration of nano ZnO is increased to 3 phr, the efficient incorporation is lacking, mainly due to the increase in the nanoparticle−nanoparticle interaction, which leads to the aggregation of ZnO nanoparticles in the matrix. The aggregated ZnO nanoparticles can be seen in the TEM image (Figure 4b) of NR-N3.

The topographic features as well as the phase characteristics of surfaces were investigated using AFM in phase contrast tapping mode. AFM images of the surface characteristics of the NR-N2 nanocomposite are given in Figure 5a−c. Figure 5a shows the three-dimensional morphology of NR-N2; the small

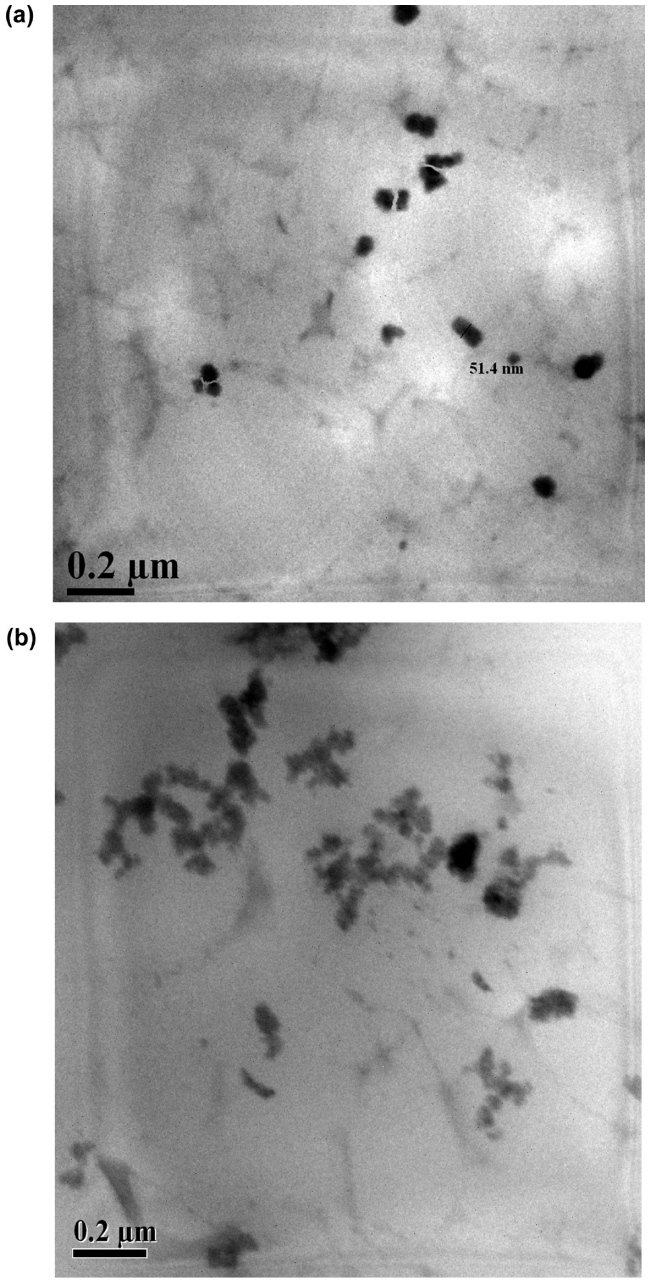

Figure 4. (a) TEM image of NR-N2. (b)TEM image of NR-N3.

heaps/hills of slightly varying dimensions on its surface indicate the presence of nano ZnO embedded in the NR matrix. The images (Figure 5a−c) show that the NR film surface is thoroughly modified, and the incorporation of nano ZnO strongly influences the film morphology. However, the distribution and the dimensions of the heaps/hills are almost homogeneous, indicating a good dispersion of nano ZnO in the polymeric matrix, suggesting that the surface of NR-N2 is clearly rougher than that of pure NR film. The more roughness of the surface indicates strong rubber−nano ZnO interaction in NR-N2. Figure 5d shows the AFM image of NR-N3, where ZnO nanoparticles are aggregated.

Dynamic Mechanical Analysis. Dynamic mechanical analysis (DMA) measures the stiffness and mechanical damping of dynamically deformed material as a function of time, temperature, and frequency. The storage modulus (E'), loss modulus (E''), and loss tangent ($\tan \delta = E''/E'$) are studied as a

dx.doi.org/10.1021/jp4039489 | J. Phys. Chem. B 2013, 117, 12632−12648

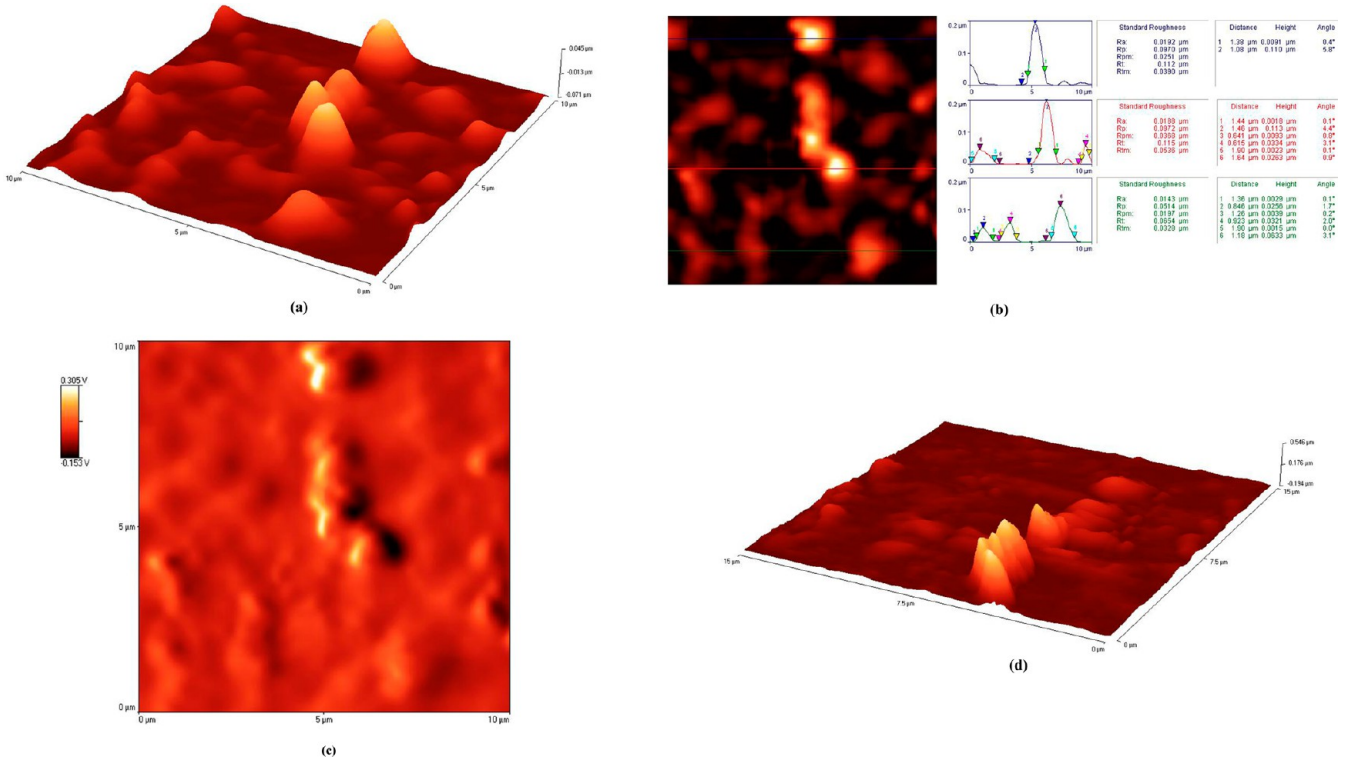

Figure 5. AFM images: (a) 3D-height, (b) height-phase, and (c) phase image of NR-N2; (d) 3D-height image of NR-N3.

function of temperature of NR nanocomposites. The storage modulus E' represents the stiffness of a viscoelastic material and is proportional to the energy stored during a loading cycle. The loss modulus E'' is proportional to the energy dissipated during one loading cycle. The loss factor tan δ is the ratio of loss modulus to storage modulus (E''/E'). It is a measure of the energy lost, expressed in terms of the recoverable energy, and represents mechanical damping or internal friction in a viscoelastic system. A high value of tan δ is indicative of a material that has a high, nonelastic strain component, whereas a low value indicates one that is more elastic. The phase angle (δ) between stress and strain is a measure of the viscous response of the material, ($\delta = 0°$ for totally elastic and $\delta = 90°$ for totally viscous). Therefore, it is clear that, when $\delta = 45°$, E' and E'' coincide with each other, and this point depends upon the applied frequency and temperature of the composites.[38] Dynamic mechanical analyses of the NR nanocomposites were carried out at three different frequencies, viz., 10, 1.0, and 0.1 Hz.

Usually, the introduction of inorganic nanofillers to a polymer matrix enhances the tan δ values of the nanocomposites as there is an enhancement in the sources of charge carriers, which is due to the increase in the effective dielectric constant and energy density in the system. The glass transition region is detected as a sudden and considerable (a decade or more) change in the storage modulus and a concurrent peak in the tan δ curve. The temperature that corresponds to the maximum of the tan δ peak is "T_g", the glass transition temperature. This shows the importance of the glass transition as a material property. It is clearly the substantial changes in the rigidity that the material experiences in a short span of temperatures.

The dual nanolayer model suggested by Tsagarapoulos et al.[39] for the properties in polymer nanocomposites is found to be suitable in explaining the behavior of the glass transition temperature T_g of nanocomposites obtained in the present study. A representative scheme is given (Figure 6a,b) for the proposed model. It was suggested that interactions between

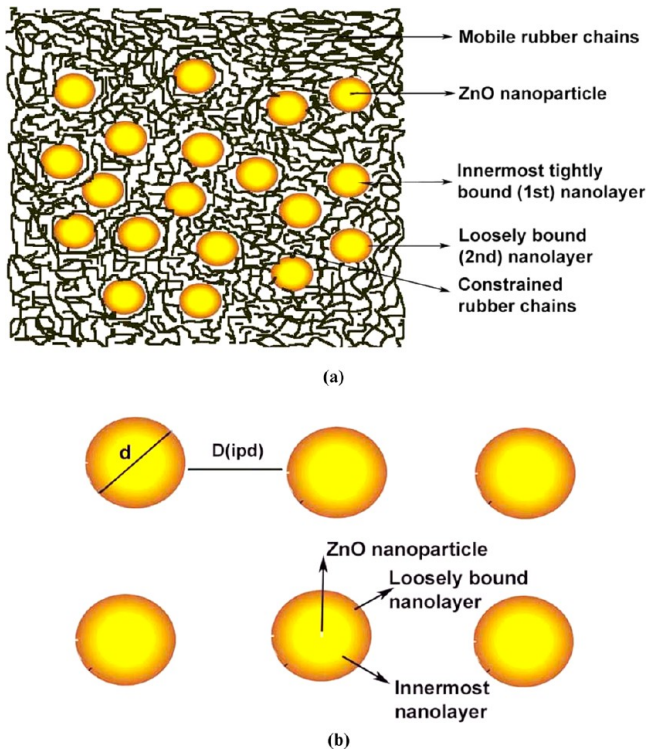

Figure 6. (a) Schematic of the core−shell morphology of rubber−nano ZnO nanocomposites. (b) Schematic of the distribution of spherical nanofiller (nano ZnO) in the rubber matrix.

dx.doi.org/10.1021/jp4039489 | J. Phys. Chem. B 2013, 117, 12632−12648

polymer chains and the highly charged nanoparticle surface actually lead to the formation of two nanolayers around the nanoparticle.[39−41] The first nanolayer very close to the nanoparticle surface (at a distance of 1−20 Å from the nanoparticle surface) is assumed to be tightly bound to the surface, resulting in the polymer chains there to be highly immobile. After that, there is the formation of a second polymer nanolayer (at a larger distance of 25−90 Å from the nanoparticle surface) with a thickness slightly more than that of the first layer, and this layer contains polymer chains that are loosely bound. Reports suggest that it is the innermost (lst) interfacial nanolayer that determines the glass transition temperature (T_g) of the nanocomposites.[39−41] These nanoparticle−polymer interactions can be attractive, repulsive, or neutral, and depending on these behaviors, T_g can increase, decrease, or remain constant. The shifting of T_g to a lower temperature region in polymer composites compared to neat polymer is due to a variety of reasons, such as changes in the molecular weight, tacticity, and cross-linking density. There is an effective constrained zone that constitutes the innermost (1st) nanolayer and the loosely bound (2nd) nanolayer, as shown in Figures 6a,b and 10, and the polymers lose their mobility during glass transition when the polymer chain is within the constrained zone. The immobility and entanglement dynamics of the polymer chains are functions of the filler concentration, and only those polymer chains that come in contact with the nanoparticles will become immobile or entangled. When these immobile nanolayers are considered for all the nanoparticles in a polymer matrix, it can be expected that the mobility of all the polymer chains interacting with these nanoparticles is restricted.

At low nanofiller concentrations (0.1−0.4 wt %), the distribution of nanofillers in the polymer is uniform with large interparticle distances, and so, the interfacial effects in nanocomposites may be much more pronounced. At low nanofiller concentrations, the mobility of loosely bound layers increases, leading to a reduction in the glass transition temperature of the nanocomposite. As the nanofiller concentration increases in the polymer matrix, the interparticle distances start to reduce, which can also result in an overlap of the immobile polymer regions around the nanoparticles, and the volume of the tightly bound layers increases. This will lead to an increase in the volume of immobile polymer regions in the nanocomposite, which, in turn, will cause an increase in the glass transition temperature, as observed in the present study. These interfacial phenomena clearly depend on nanofiller dispersion in the nanocomposites. The synthesis of nanocomposites, which are completely free from aggregation at high nanofiller concentrations, is difficult. The interfacial phenomena occurring at aggregated or clustered nanofiller locations are difficult to comprehend using the proposed model.

The graphical representation of the variation of storage modulus with temperature of neat NR and NR nanocomposites at 10 Hz is shown in Figure 7. The plot of log E' versus temperature (Figure 7) gives nice information about the shift in the glass transition and the increase in the storage modulus at the high-temperature region compared to neat NR. There is a large fall in the modulus with increasing temperature in the unfilled system. The storage modulus of neat NR drops from ~10^5 to ~10 MPa in the glass transition region; it is due to the fact that, in the glassy state, molecular motions are largely restricted to vibration and short-range rotational motions. Increasing the amount of nano ZnO successively increases the

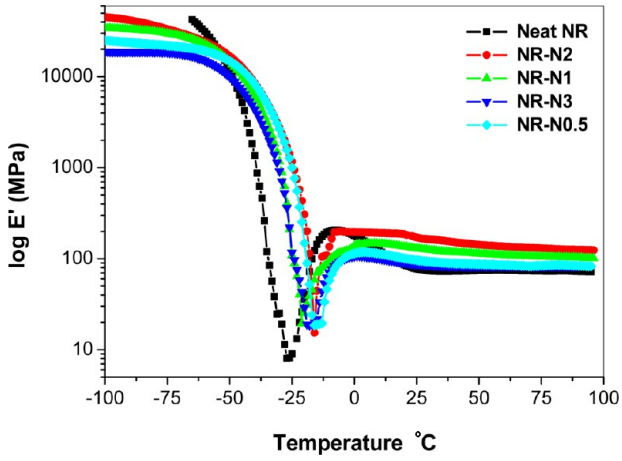

Figure 7. Plot of log E' vs temperature of NR nanocomposites.

values of E', and the highest modulus is observed for the composite containing 2 wt % of nano ZnO. This kind of enhancement in the modulus can be observed even below the glass transition temperature. The increase in T_g upon the addition of nano ZnO could be easily understood from the midpoint (T_g) of the transition of the storage modulus curve. A sharp modulus drop appears for all samples in the glass−rubber transition zone. This modulus drop is mainly due to the energy dissipation in the relaxation process where tan δ is maximum at this point. This relaxation process mainly depends on the cooperative motions of long chain sequences. Above T_g, the modulus becomes roughly constant over a wide temperature region called the rubbery plateau region in the case of composites having high nanofiller loading. In the case of unfilled NR and low filler content composites, the rubbery modulus is known to depend on the degree of crystallinity of the material. The increase in the glass transition temperature indicates the enhanced degree of reinforcement upon the addition of nano ZnO in the NR matrix. It can also be noted that the storage modulus increases marginally with the addition of nano ZnO; the changes are very clear between 25 and 80 °C. This is a clear indication of the homogeneous dispersion of nano ZnO in the NR matrix. It emphasizes that there is the existence of good rubber−nano ZnO interaction, and the reinforcement in the presence of nano ZnO is moderately strong there by restricting the mobility of the chain segments. It was found that incorporation of nano ZnO increases the storage modulus and loss modulus and exhibits the best mechanical stiffness.

The effectiveness of fillers on the moduli of the composites can be represented by a coefficient "β_f", which is expressed as[42]

$$\beta_f = \frac{(E_g'/E_r')\ \text{nanocomposite}}{(E_g'/E_r')\ \text{rubber}} \tag{10}$$

where E'_g and E'_r are the storage modulus values in the glassy and rubbery regions, respectively. The low value of β_f shows the higher effectiveness of the nanofiller. The β_f values calculated for all the nanocomposites at a frequency of 10 Hz are given in Table 5. The effectiveness of the nanocomposites is gradually increasing with filler content, and the highest effectiveness is observed for NR-N2. It is important that the modulus in the glassy state is determined primarily by the strength of the intermolecular forces and the way the polymer chains are arranged. At high temperature, the stiffness is determined by

dx.doi.org/10.1021/jp4039489 | J. Phys. Chem. B 2013, 117, 12632−12648

Table 5. Theoretical Predictions of Storage Modulus and "β_f" Values

sample	rule of mixtures model (GPa)	Einstein model (GPa)	Guth model (GPa)	experimental (GPa)	"β_f" values
NR-Neat	13.72	13.72	13.72	13.72	1.00
NR-N0.5	13.79	13.89	13.81	13.98	0.51
NR-N1	13.92	14.06	13.94	14.11	0.46
NR-N2	14.06	14.40	14.13	14.76	0.29
NR-N3	14.12	14.72	14.12	9.54	0.57

the amorphous regions, which are very flexible above the relaxation transition. The equation for the prediction of storage modulus of the nanocomposite by the inclusion of nanofiller is the rule of mixtures, and it is given by the equation

$$E'_c = E'_m(1 + \nu_1) \quad (11)$$

where E'_c and E'_m are the storage moduli of the nanocomposite and rubber matrix, respectively. Einstein had modified this model with an adhesion parameter, and Einstein's model is given by the equation

$$E'_c = E'_m(1 + 2.5\nu_1) \quad (12)$$

where 2.5 is the adhesion parameter featuring good adhesion, and ν_1 is the volume fraction of the nanofiller. This model has been used to investigate the adhesion between the spherical filler and an incompressible matrix and is valid only at low concentration of filler particles. Later, Guth has modified this equation, considering a higher degree of physical and chemical interactions between the filler and the polymer. The Guth equation is

$$E'_c = E'_m(1 + 1.25\nu_1 + 14.1\nu_1^2) \quad (13)$$

The experimental and theoretical moduli values are given in Table 5. It can be seen that the experimental values are greater than the theoretical values of the three models studied. Guth equations are used for modeling composites, where there is chemical interaction between filler and polymer. Among the three models studied, the Einstein model suits with the experimental values of storage modulus. Table 5 (columns 2−5) signifies the better level of interfacial interaction and adhesion between the nanofiller and the NR matrix.[43] It was clear that, for NR-N3, none of the models agree with the experimental value of storage modulus and the calculated "β_f" value is very high compared with other samples. These points firmly indicate that there is aggregation of ZnO nanoparticles in NR-N3.

tan δ Peak. The magnitude of the tan δ peak value depends on the nature of the polymer system, and the tan δ peak value signifies the dissipation of energy due to internal friction and molecular motions. The tan δ peak value decreases with increasing nanofiller content for the NR nanocomposites, as shown in Figure 8. The damping peak occurs in the region of glass transition, where the material changes from rigid to a more elastic state and is associated with the movement of small groups and chains of the molecule within the polymer structure, all of which are initially in a frozen state. The damping is affected through the incorporation of fillers in a composite system. This is mainly due to shear stress concentrations at the filler surface in association with additional viscoelastic energy dissipation in the matrix. In the present case, the nanofiller particles are distributed homogeneously in the NR matrix, so

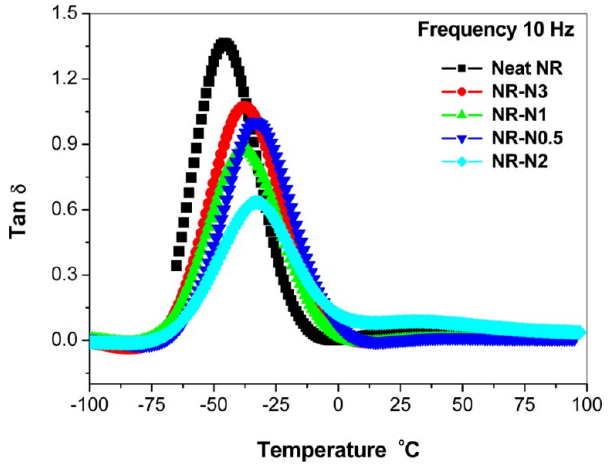

Figure 8. Plot of tan δ vs temperature of NR nanocomposites.

the shear stress is uniformly distributed throughout the nanocomposites. The lowering of tan δ peak values of the NR nanocomposites can be ascribed to the confinement of NR chains by nano ZnO, and this confined fraction changes with varying weight % of nano ZnO. A similar behavior has been reported for other micro- and nanocomposites. The lowering of tan δ peak values are indicative of an improvement in the interfacial reinforcement in the nanocomposites. The damping at the interfaces depends upon the force of adhesion between nano ZnO and NR. At high nanofiller content, when strain is applied to the nanocomposite, the strain is controlled mainly by the filler in such a way that the interface, which is assumed to be the more dissipative component of the composite, is strained to a lesser degree.[44]

In the present case, the "T_g" of the nanocomposites is found to be shifted toward higher temperature as compared to that of neat NR with respect to the weight % of nano ZnO, as shown in Figure 8. It was also observed that the addition of more weight % of nano ZnO (up to 2 phr) resulted in the broadening of the peak and also the decrease in the magnitude of the tan δ peak, indicating the restricted mobility of polymer chains and the broader distribution of relaxation times in the NR nanocomposites.[45] Further addition of nano ZnO, that is, 3 phr, causes aggregation of ZnO nanoparticles in the matrix. In an unfilled system, the polymer chain segments are free from restraints and have enough mobility. The addition of nanofillers show a positive shift of the "T_g" values, showing the effectiveness of the nanofiller as the reinforcing agent. The shifting of "T_g" to higher temperature can be associated with the decreased mobility of the polymer chains by the addition of nanofillers and the increased interfacial reinforcements between nanoparticles and the matrix.[46] The glass transition temperature of the amorphous polymers can vary widely with the chemical structure of the repeating unit of the polymer chain, the flexibility of the polymer chain, and the nature and morphology of the nanofiller. In various frequency (10, 1.0, 0.1 Hz) measurements, it is seen that the glass transition temperature of the nanocomposites is found to be shifted toward higher temperature as compared to the neat NR with respect to the weight % of nano ZnO.

Theoretical Predictions of tan δ. The damping property of a composite results from the inherent damping of the constituents. Rigid fillers usually lower the damping behavior. The damping can be represented as

dx.doi.org/10.1021/jp4039489 | J. Phys. Chem. B 2013, 117, 12632−12648

$$\tan \delta_c = V_f \tan \delta_f + V_m \tan \delta_m \quad (14)$$

where the subscripts "c" and "m" represent the composite and matrix, V_m is the volume fraction of the matrix, and V_f that of the filler. However, in the case of rigid particulate fillers sintered at a high temperature, the first term in the right-hand side can be neglected because "δ_f", the loss factor for nano ZnO, is zero at 150 °C, the cure temperature of the NR nanocomposites, and therefore, eq 14 becomes

$$\tan \delta_c = V_m \tan \delta_m \quad (15)$$

However, this equation has taken into account the variation in the modulus of the nanocomposite resulting from the differences in the processing conditions. This is mainly due to the stiffness or additional constraints imposed on the matrix and is similar to the increased stiffness of the layer covering the nanoparticle. By the proposed model (Figure 6a,b), we can believe that the layer surrounding the nanofiller particle is denser than normal NR, and this, in turn, can further reduce the tan δ values. Therefore, eq 15 should contain a stiffness term. It is assumed that the presence of nanofillers in the matrix can provide stiffness, which is equivalent to the minimum elastic modulus of the nanocomposite, and the above equation can be modified as[47]

$$\tan \delta_c = V_m \left(\frac{E'_m}{E'_c} \right) \tan \delta_m \quad (16)$$

McNally et al.[48] have reported that, at lower frequencies, the decrease in tan δ is much more than at higher frequencies. It can be observed from Figure 8 that, as the weight % of nano ZnO increases, the broadening of the tan δ peak becomes more pronounced. The observed reduction in tan δ peak height is attributed to the presence of an interfacial interaction between the NR matrix and nano ZnO. This is also due to the increased hindrance for energy dissipation and relaxation of NR chains in the presence of nano ZnO.

Area under tan δ Peak. Dynamic mechanical analysis (DMA) is used to study the polymer chain mobility of composites at the glass transition region. The lowering of the tan δ peak (Figure 8) indicates the reduction in the number of mobile chains during glass transition; that is, a significant portion of polymer chains become immobilized or entangled in the nanocomposite in the presence of nano ZnO. The area under the experimental tan δ peak can be obtained from the graph (Figure 8) by integration. The relative peak height or area is proportional to the volume of the constrained polymer chains (V_{con}). The area under the tan δ peak (experimental and theoretical) is plotted along with the weight % of nano ZnO, as given in Figure 9a. From Figure 9a, we have calculated the ratio of theoretical area to experimental area. It is assumed that, if there is no immobilized layer between the nanofiller and the polymer, the ratio should be 1. From Figure 9a, it is noted that the immobile region is proportional to the volume of constrained polymer chains; that is, the ordinate of the graph representing the ratio of area under the theoretical tan δ to the experimental tan δ is proportional to V_{con} (Figure 9b). The graph shows a linear relation to the weight % of nano ZnO; however, the immobility and entanglement dynamics of the polymer chains are functions of the nanofiller concentration. For NR-N0.5, NR-N1, and NR-N2, the value of the area under the theoretical tan δ is higher than the area under the experimental tan δ (Figure 9a). Since the ratio of the area under the theoretical tan δ to the area under the experimental tan δ is

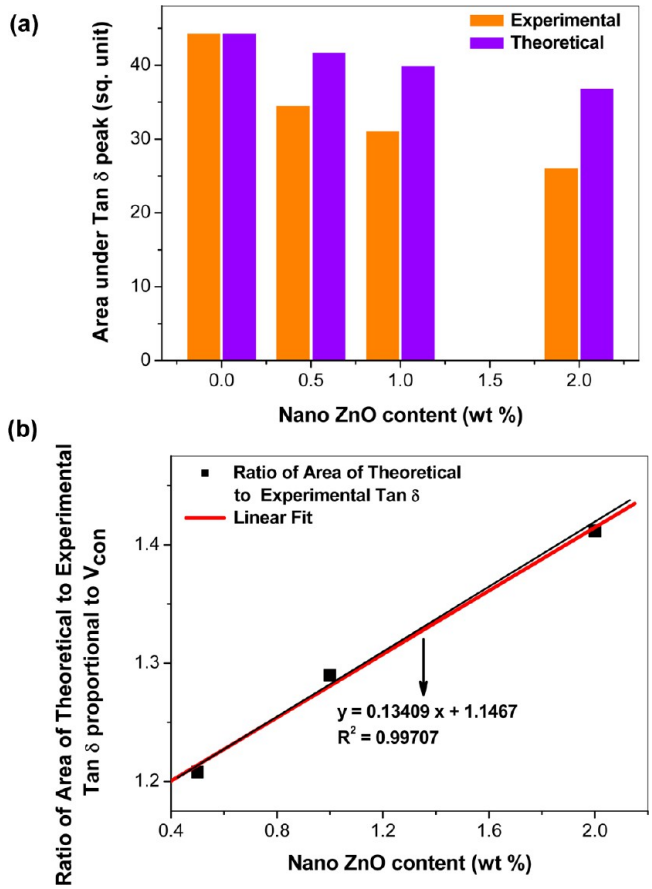

Figure 9. (a) Area under tan δ peak vs nano ZnO content (wt %). (b) Ratio of area of theoretical tan δ to experimental tan δ vs nano ZnO content (wt %).

proportional to the volume of constrained rubber chains V_{con}, the volume of the constrained rubber chains increases with increasing weight % of nano ZnO in a linear manner, and the data points are best fit by a linear equation in Figure 9b. That is, as the weight % of nano ZnO increases, the segmental motion of more rubber chains is progressively restricted, and thus, the volume of the constrained rubber chains increases. During the preparation of nanocomposite itself, the nanoparticles adhere with the polymer and a rigid amorphous layer is formed around the nanoparticle. As the weight % of nano ZnO increases, it is natural to form more of such a rigid portion. The surface-to-volume ratio is very high for nanoparticles compared to microparticles, and there are more chances for adhering more polymer chains to nanoparticles. The linear fit of the plot (Figure 9b) shows that V_{con} is directly proportional to the weight % of nano ZnO, and V_{con} will depend not only on the nano ZnO content but also on the nature of the polymer−filler interaction. Since the relative peak height or area is proportional to the volume of the constrained polymer chains, eq 16 supports our proposed structural model and core−shell morphology. According to Figure 9b

$$V_{con} \propto \text{ weight \% of nano ZnO} \quad (17)$$

Constrained Polymer Region in NR Nanocomposites. As discussed above, during the glass transition, the long-range polymer chains gain mobility and thus dissipate a great amount of energy through viscous movement. This is shown in the tan δ peak (Figure 8). This maximum point of the tan δ peak was

dx.doi.org/10.1021/jp4039489 | J. Phys. Chem. B 2013, 117, 12632−12648

very sensitive toward the parameters, such as filler content or morphology, than T_g itself.[49] The lowering of the tan δ peak indicates that there is a reduction in the amount of mobile polymer chains during the glass transition and hence can be used to estimate the amount of constrained chains.[45] It was also observed that the broadening of the tan δ peak and the lowering of the peak height indicate the restricted mobility of polymer chains in the NR nanocomposites.[45] To understand the role of the constrained region in enhancing the mechanical properties of the nanocomposites, it is important to determine the volume fraction of these regions in NR nanocomposites. For this, we have proposed a constrained polymer model (Figures 10 and 6a).

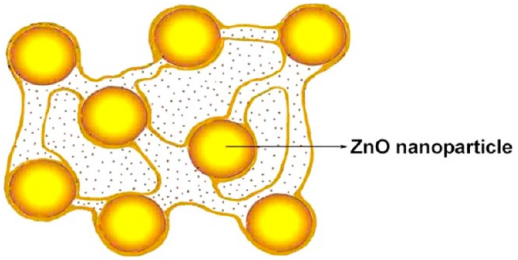

Figure 10. Constrained polymer model. The dotted area represents the constrained rubber region around each ZnO nanoparticle.

For linear viscoelastic behavior, the relationship between the energy loss fraction of the polymer nanocomposite W and tan δ is given by the following equation[50]

$$W = \frac{\pi \tan \delta}{\pi \tan \delta + 1} \tag{18}$$

The energy loss fraction W at the tan δ peak is expressed by the dynamic viscoelastic equation

$$W = \frac{(1 - C_v)W_0}{(1 - C_0)} \tag{19}$$

where C_v is the volume fraction of the constrained region, $(1 - C_v)$ is the fraction of the amorphous region, and W_0 and C_0 represent the energy fraction loss and volume fraction of the constrained region for pure NR, respectively. This equation can be rearranged as

$$C_v = 1 - \frac{(1 - C_0)W}{W_0} \tag{20}$$

The energy loss fraction at the tan δ peak is obtained at the frequency of 10 Hz, and the value of C_0 is taken to be 0 (totally amorphous phase in NR matrix). The height of the tan δ peak is used to calculate W according to eq 18.[50−52] The fraction of the constrained region of NR nanocomposites can then be calculated from eq 20 (Table 6, column 5). The homogeneous dispersion of nano ZnO generates a larger contact area between the nano ZnO and rubber chains and hence the enhanced interfacial attraction between nano ZnO and rubber chains; this will result in a larger amount of the constrained region. The volume fraction of the constrained region C_v of the nanocomposites increases with the addition of nano ZnO, and the value is highest for the sample NR-N2. Further addition of nano ZnO (3 phr) causes aggregation of nanoparticles and very poor interfacial interaction between nano ZnO and rubber chains, and hence, the C_v value is very low. Figure 11 shows a

Table 6. Tensile Strength, Tensile Modulus, Elongation at the Break, and Estimated Volume Fraction of the Constrained Rubber Region

sample	tensile strength (MPa)	tensile modulus (MPa) 300%	elongation at break (%)	volume fraction of the constrained rubber region (C_v)
NR-N0.5	11.58	0.57	1497	0.0631
NR-N1	18.17	0.87	1403	0.0947
NR-N2	25.56	2.28	637	0.1760
NR-N3	6.68	1.37	873	0.0484

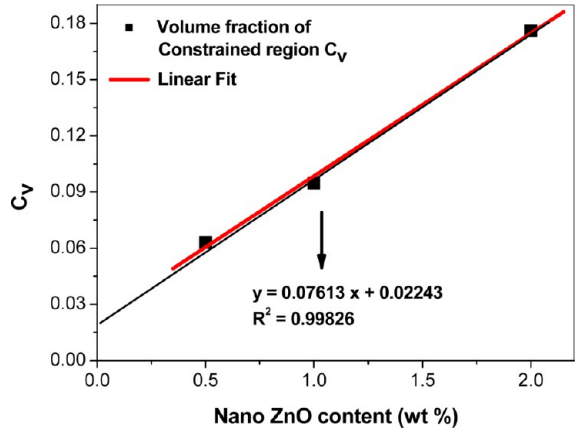

Figure 11. Plot of C_v vs nano ZnO content (wt %).

linear relationship between C_v and weight % of nano ZnO. This indicates that the fraction of the constrained region in a polymer nanocomposite will depend on the filler content, the nature of the polymer, and the nature of the polymer−filler interactions. According to Figure 11

$$C_v \propto \text{ weight \% of nano ZnO} \tag{21}$$

Both Figures 9b and 11 show that the volume of the constrained region is directly proportional to the weight % of nano ZnO. Equations 16 and 20 firmly support our core−shell morphology model and constrained polymer model, because, by both of them, the volume of the constrained region is in direct proportion to the weight % of nano ZnO.

It was reported by many researchers that a small amount of nanofiller is sufficient to immobilize a significant portion of polymer chains during the glass transition.[16,50,51,53,54] Therefore, it can be seen that such significant differences in the value of C_v can be attributed to the nature of the polymer, whether it is amorphous, semicrystalline, or cross-linked rubber. For a comparative study of the quantity of the constrained volume in various nanocomposites, we have checked the DMA measurements of various nanocomposites in the literature. DMA measurements gave very nice information about the variation in the constrained volume in different nanocomposites. Pochan et al.[53] have observed that the addition of 5 wt % of nanoclay in an intercalated latex copolymer resulted in an increase in the constrained volume from 0 to 50%. Utracki et al. reported[54] that the incorporation of 1.6 wt % of nanoclay reduced the free volume percentage by 14% in the exfoliated nylon 6/nanoclay system, and only a 5% volume reduction was observed in the intercalated PS/nanoclay nanocomposites containing 4 wt % of nanoclay.[54] Loo et al.[55] have observed that, in polymer nanocomposites based on completely amorphous poly(hexamethylene isophthalamide)/clay nanocomposites, for 5 wt % of

dx.doi.org/10.1021/jp4039489 | J. Phys. Chem. B 2013, 117, 12632−12648

MMT in the polymer matrix, the increased volume percentage of the constrained region (<9%) was much less than those of nylon 6/clay (30% for 5 wt % of clay)[54] and latex/clay (50% for 5 wt % of clay)[53] systems, but are quite close to that of the PS/nanoclay hybrid (5% caused by 4 wt % of clay).[54] Loo et al.[55] have also reported that, in poly(hexamethylene isophthalamide)/clay nanocomposites, more constrained region exists in the exfoliated nanocomposites than that of the intercalated one, and their investigations give a very informative finding that the constrained volume in amorphous polymer nanocomposites was found to be much less than that in semicrystalline systems. We have compared the volume fraction of the constrained region in NR-nano ZnO nanocomposites in the present study with that of our previously reported prevulcanized NR latex–nano ZnO nanocomposites[16] and found that the volume fraction of the constrained region in the present study is less than that of our previous report for the same weightt % of nano ZnO. Our proposed model helps to explain this difference. Figure 10 shows the nature of the constrained region in an amorphous polymer in the vicinity of ZnO nanoparticles. The low volume of the constrained region is composed of the proximal polymer chains encircling nano ZnO, as shown in Figure 10. Furthermore, the dispersion of nano ZnO in the polymer matrix depends on the morphology of nano ZnO; better dispersion would result in the higher volume of constrained polymer segments. That is the reason for the existence of more constrained region in NR-N2 nanocomposite than in NR-N0.5. It indicates that the degree of nanofiller dispersion and interactions between the nanofiller and polymer chains are crucial in determining the microstructure of the amorphous polymer nanocomposites.[53,56] It was reported that, in rubber–clay nanocomposites,[57] the addition of nanoclay has strongly affected the crystallization process and crystallite size in the cross-linked rubber.

Mechanical Properties. Next, we focus our attention on studying the variation of the tensile strength of rubber nanocomposites by gradually increasing the nano ZnO content. The stress–strain behavior of rubber nanocomposites was studied at room temperature. From the stress versus strain curves, it was observed that, for rubber nanocomposites, initially, the stress increases very slowly, and after a particular value of strain (above 300%), the tensile stress increases rapidly and reaches the maximum. This clearly shows that the strain-induced crystallization operates in all the rubber nanocomposites. Table 6 shows the tensile strength, tensile modulus, and elongation at the break of rubber nanocomposites. The tensile strength and tensile modulus increase with the addition of the nano ZnO content from 0.5 to 2 phr and decrease on further addition of nano ZnO. The tensile strength and tensile modulus are maximum for NR-N2. The elongation at break of rubber nanocomposites decreases with the increase in nano ZnO content from 0.5 to 2 phr and increases on further addition of nano ZnO. A comparison of the reported value of the NR–micro ZnO filled composite[37] shows that about 27% enhancement in the tensile strength, 78% enhancement in the modulus (300%), and 48% decrease in the elongation at the break for the NR-N2 nanocomposite. The decrease in the value of tensile strength and tensile modulus and the increase in the value of the elongation at the break for the addition of 3 phr of nano ZnO is due to the aggregation of nanoparticles at higher concentration.

Influence of Interparticle Distance and Surface Area in Reinforcement Mechanism. The main reinforcement mechanism in rubber nanocomposites can be generally attributed to rubber–nanofiller and nanofiller–nanofiller networking interactions. The rubber–nanofiller interactions directly depend on the structure and surface activity of the nanofiller, which results in the formation of a physical rubber–nanofiller network or increased cross-linking density,[58] or the formation of the bound rubber,[59] or even glassy polymer layers around the nanofiller surface.[60] Meanwhile, Sternstein et al.[8] have found that the primary underlying mechanism for reinforcement and nonlinear behavior (Payne effect) is attributed to filler–matrix interactions, such as trapped entanglements, rather than filler agglomeration or percolation. Through the surface activity of fillers, filler–filler interactions are also possible, which results in the formation of occluded rubber confined in the filler networks.[61] Strain amplification or hydrodynamic reinforcement involves the stiffening of the elastomeric matrix upon addition of hard fillers, such as carbon black. Furthermore, the reinforcement also greatly depends on the thermodynamic state of the polymer matrix.

The process of alignment and orientation of NR chains during the tension and retraction of the nanocomposite is described in Figure 12. In rubber nanocomposites, stretching and parallel-arraying of rubber chains induced by the nanofillers are formed during stretching. The distance between neighboring nanofiller particles should be small enough, and the cross-linked chains can be attached to at least two nanofiller particles

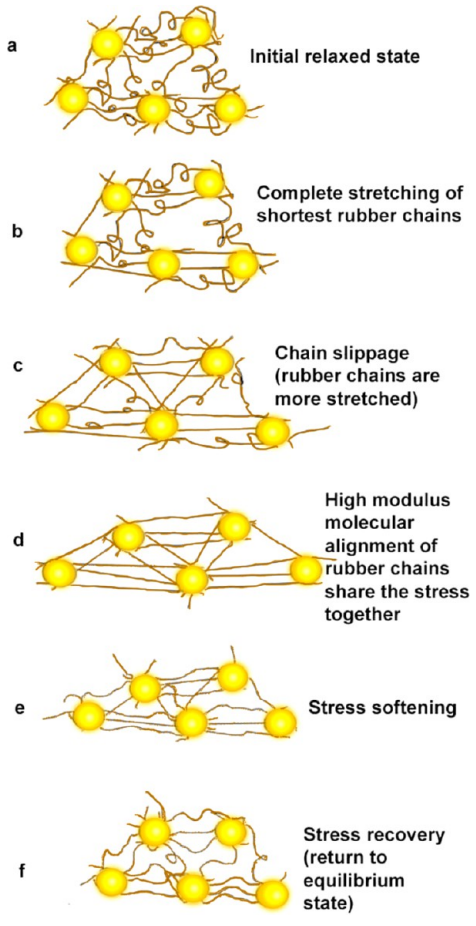

Figure 12. Schematic of stretching and parallel-arraying of rubber chains in NR–nano ZnO nanocomposites during stretching and retraction.

at the same time (like chain bridges). This interparticle distance is directly related to the nanofiller loading and also depends greatly on the dispersion state and particle size. In the case of a large interparticle distance (i.e., low nanofiller loadings), the chain bridges cannot be formed or just have fewer chains attached to the nanofillers so that many parallel alignments of straightened chains, by the slippage of polymer chains on the nanoparticle surface during tension, will not appear, which corresponds to the very low strength. At high nanofiller loadings (not the case of aggregation), more and more straightened and parallel polymer chains induced by the nanofillers are formed, and as a result of this process, the interparticle distance will be less. However, to quantify accurately the distance between nanoparticles in nanocomposites is very difficult. The literature reports suggest that two main methods, such as small-angle neutron scattering[62] and 3D-TEM methods,[63] were employed to measure the average distance between nanofillers in nanocomposites. However, these methods need assisted instruments, and also due to the nonavailability of these instrumental techniques, we have proposed a model to calculate the average distance between nanoparticles, which is shown in Figure 6b. When spherical nanoparticles are homogeneously distributed in a polymer matrix, the interparticle distance D_{ipd} between two nanoparticles is calculated by using the equation[64]

$$D_{ipd} = r\left[\left(\frac{4\pi}{3\nu}\right)^{1/3} - 2\right] \tag{22}$$

where r is the radius of the ZnO nanoparticle, the diameter d of the ZnO nanoparticle was obtained from HRTEM images,[16] and ν is the volume fraction of the nanoparticle. Previously Wu[65] had used this model to calculate the average distance between rubbery particles for the investigation of the toughness of plastics and also put forward the concept of critical particle−particle distance (CPD) for the toughness of plastics. Zhang et al.[66] have also used this model to study the percolation phenomena and mechanism of strengthening of elastomers, viz., SBR and EPDM, by incorporating nanofillers, such as carbon black and nano ZnO, respectively, and proposed the concept of CPD to explain the observed percolation phenomenon and mechanism of strengthening of the elastomer matrix in the studied nanocomposites.

It is also possible to calculate the surface area of nanoparticles S per unit volume of the nanocomposite by the following equation[67]

$$S = \frac{3\nu}{r} \tag{23}$$

where ν is the volume fraction of the nanoparticle and r is the radius of the ZnO nanoparticle. Since the nanoparticles have a large surface area, the interaction zones in a nanocomposite are much larger than those in a polymer containing microparticles. The surface region formed by nanoparticles (and, consequently, the interfacial surface region) in nanocomposites is 3 orders of magnitude larger than that formed by the microparticles in microcomposites.

In the present study, we have observed from SEM and HRTEM images that the dispersion of nano ZnO in the rubber matrix is consistent with the homogeneous dispersion, as shown in Figure 6a,b. The interparticle distance (D_{ipd}) as a function of volume fraction of nano ZnO can then be calculated by using eq 22, and the result is shown in Figure 13a. The

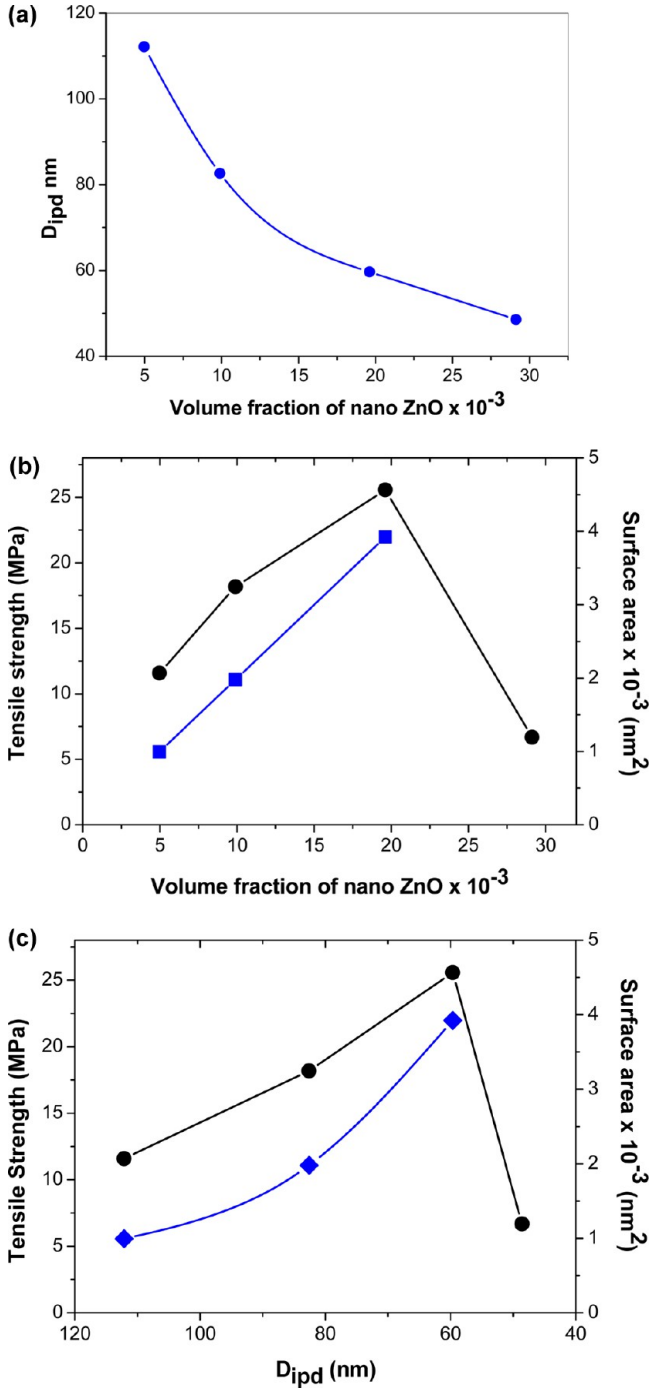

Figure 13. (a) Plot of D_{ipd} vs volume fraction of nano ZnO. (b) Variation of tensile strength and the surface area of ZnO nanoparticles per unit volume of the nanocomposites with respect to volume fraction of nano ZnO: (black circle) tensile strength, (blue square) surface area. (c) Variation of tensile strength and the surface area of ZnO nanoparticles per unit volume of the nanocomposite with respect to D_{ipd}: (black circle) tensile strength, (blue square) surface area.

figure indicates that the interparticle distance decreases gradually with increasing the volume fraction of nanoparticles, exhibiting a nonlinear relationship. Replacing the volume fraction of nano ZnO with the corresponding calculated theoretical interparticle distance (Figure 13b), we get the relationship between the tensile strength, surface area of ZnO nanoparticles S per unit volume of the nanocomposite, and the

dx.doi.org/10.1021/jp4039489 | J. Phys. Chem. B 2013, 117, 12632−12648

theoretical interparticle distance, as shown in Figure 13c. Figure 13c shows that the tensile strength and the surface area of ZnO nanoparticles S per unit volume of the nanocomposite increase with the decrease in interparticle distance and reach a maxmium value up to a particular value of the interparticle distance, and after that, they decrease. Since the incorporation of 3 phr of nano ZnO causes aggregation of nanoparticles in the NR matrix, the surface area of nanoparticles S per unit volume of the nanocomposite decreases. This observation indicates that there exists a CPD of nano ZnO in the rubber matrix for homogeneous dispersion, and hence, the resulting nanocomposite exhibits a moderately strong rubber−nanofiller interaction, which brings good tensile strength of the nanocomposite. The relationship between tensile strength and theoretical interparticle distance supports the proposed model. When nanoparticles approach the CPD, each polymer chain can be adsorbed onto two or more neighboring nanoparticles, and the formation of straightened polymer chains by slipping on the particle surface during deformation is possible.

Factors Affecting Rubber−Nanofiller Interaction in the Present Study. *The Influence of Dispersion.* The dispersion of nanoparticles is very crucial in the polymer matrix in the formation of nanocomposites. The formation of nanoparticle aggregates in the polymer matrix will reduce their ability to physically adsorb the rubber chains onto their surface. Accordingly, the interparticle distance will be large, and this adversely affects the tensile strength of the resulting nanocomposite. The homogeneous dispersion of nanoparticles in the polymer matrix is always advisable for good polymer−filler interaction and hence the improvement of mechanical properties compared to conventional microfillers. In the present study, homogeneous dispersion of nano ZnO in NR is observed in the HRTEM images of 0.5, 1.0, and 2.0 phr of nano ZnO and incorporation of more weight % of nano ZnO, that is, 3 phr, in the NR matrix causes aggregation of ZnO nanoparticles, and this will reduce the cross-link density and mechanical properties of the resulting nanocomposites, as explained in Figure 2 and Table 6, respectively.

Size of the Fillers and Interfacial Adhesion between Rubber and Fillers. The size of the fillers and their type of interaction with the rubber matrix play an important role in determining the properties of rubber composites. Usually, the size of the filler used for rubber strengthening is always very small; the nanofillers have a large specific surface area, strong surface activity, strong adsorption capability, and better matrix strengthening compared with microfillers. The interparticle distance D_{ipd} is related to the size and weight % of the filler. In this study, Figure 13a shows that the D_{ipd} decreases with the increase in weight % of nano ZnO for a given particle size. In the case of microfillers, the interparticle distance increases with the size of the filler. It is generally considered that the critical particle distance (CPD) might be larger than the size of the polymer chain in the real system. Considering the theoretical aspect, when filler particles approach such a critical distance, each polymer chain can be adsorbed onto two or more neighboring filler particles by the formation of straightened polymer chains by slipping on the filler particle surface during shear or tension. In the case of the nano ZnO filled NR matrix, we expect that the system has continuous networks with straightened rubber chains by slipping on the filler particle surface during deformation; however, it was believed that the number of straightened rubber chains formed in the deformed state was more in the NR-N2 than the NR-N0.5 nanocomposite. This might be due to the reason that the number of straightened rubber chains is related to the total surface area of the interface between the filler and rubber. It was understood that the total surface area of the interface between rubber and nano ZnO is much larger in the NR-N2 nanocomposite. The type of interaction between rubber and ZnO contains no chemical bonding between them. Furthermore, ZnO mainly exhibit physical adsorption with the elastomer due to its inorganic nature. Hence, we believe that a kind of physical adsorption between rubber chains and nano ZnO is possible. Nano ZnO has a large surface area and high surface activity, which leads to stronger adsorption on the rubber chains and better strengthening, and the resulting nanocomposites exhibit a moderately strong rubber−filler interaction, hence the enhancement in the mechanical properties.

Cross-Link Density. The experimental results explained in this study directly support that there exists an optimum cross-link density for the system. At that state, the rubber chains are easier to align among the nanoparticles, as explained before, and the tensile strength is maximum at that particular value of cross-link density. From Figure 2, it was clear that the cross-link density slowly increases and reaches a maxmium value for NR-N2, and after that, it decreases for NR-N3 due to aggregation of ZnO nanoparticles in the matrix, showing that there is an optimum cross-link density for the system. The tensile strength is maximum for NR-N2 among all other nanocomposites.

4. CONCLUSIONS

On the basis of the above results and discussion, it has been observed that the addition of nano ZnO (0.5−2 phr) in NR increases the volume fraction of the constrained region, the cross-link density, decreases the porosity, diffusion coefficient, and oxygen permeability due to a decrease in the free volume cell size and fractional free volume. The addition of 3 phr of nano ZnO in NR causes aggregation of particles. All the NR nanocomposites exhibited strain-induced crystallization. The tensile strength and tensile modulus of NR nanocomposites significantly increased by the addition of 0.5−2 phr of nano ZnO, and the value is maximum for NR-N2. However, there was significant enhancement in mechanical properties and the gas barrier property of the nanocomposite (NR-N2) due to moderately strong rubber−nanofiller interactions.

We have studied in detail the structure−property relationship of the NR−nano ZnO nanocomposite system. The dynamic mechanical properties of nano ZnO reinforced NR composites are greatly dependent on the volume fraction of the filler. The glass transition temperature T_g of NR nanocomposites is shifted toward the higher-temperature region on the addition of nano ZnO, justifying the homogeneous dispersion of nano ZnO in NR, as revealed by SEM, HRTEM, and AFM analysis. The larger surface area of ZnO nanoparticles can bring a strong interfacial interaction between the two phases, and thereby reduce the mobility of rubber chains in the proximity of nanoparticles. We have studied the nature and role of the constrained polymer region in the reinforcement mechanism by proposing a constrained polymer model. The type of polymer−nanofiller interaction strongly influences the quantity and modulus of the constrained polymer region, which, in turn, contributes to the enhancement in the storage modulus of the polymer nanocomposite. The interfacial adhesion plays a major role in determining the interactions between the rubber chains and the ZnO nanoparticles and the formation of immobilized

or constrained rubber chains in the proximity of ZnO nanoparticles. The quantity of constrained rubber shows a linear relationship with the weight % of nano ZnO. It was also studied that the main reason for effective strengthening of rubber chains is attributed to the stretching and parallel alignment of rubber chains induced by nanofillers in the process of tension. Finally, it was observed that the homogeneous dispersion of nanoparticles, the interfacial interaction between rubber and nanofillers which contain partial physical adsorption rather than complete chemical bonding is essential and an optimum cross-linking density of the system are essential for effective rubber−filler interactions in the NR matrix.

■ ASSOCIATED CONTENT

Supporting Information

Cure characteristics at 150 °C of NR nanocomposites. This material is available free of charge via the Internet at http://pubs.acs.org.

■ AUTHOR INFORMATION

Corresponding Author

*E-mail: bindu_patanair@yahoo.com, bindup001@yahoo.com.

Notes

The authors declare no competing financial interests.

■ ACKNOWLEDGMENTS

P.B. thanks the Department of Science and Technology (DST), New Delhi, India, for the award of the Young Scientist Fellowship and financial assistance for carrying out the research project. We thank Prof. Subhadra Patanair, Former Head, Department of Mathematics, S. N. M. College Maliankara, Ernakulam, India, for valuable discussions and suggestions in the theoretical modeling.

■ REFERENCES

(1) (a) Roberts, A. D., Ed. *Natural Rubber Science and Technology*; Oxford University Press: Oxford, U.K., 1988. (b) Mark, J. E.; Erman, B.; Eirich, F. R. *Science and Technology of Rubber*; Academic Press: San Diego, CA, 1994. (c) Gent, A. N., Ed. *Engineering with Rubber: How to Design Rubber Components*; Carl Hanser Verlag: Munich, 2001. (d) White, J. R., De, S. K., Eds. *Rubber Technologist's Handbook*; Rapra Technology Ltd.: Shrewsbury, U.K., 2001.

(2) (a) Tanaka, Y. *Rubber Chem. Technol.* **2001**, *74*, 355. (b) Karino, T.; Ikeda, Y.; Yasuda, Y.; Kohjiya, S.; Shibayama, M. *Biomacromolecules* **2007**, *8*, 693.

(3) (a) Mandelkern, L. *Rubber Chem. Technol.* **1993**, *66*, G61. (b) Magill, J. H.. *Rubber Chem. Technol.* **1995**, *68*, 507. (c) Toki, S.; Fujimaki, T.; Okuyama, M. *Polymer* **2000**, *41*, 5423.

(4) Takahashi, Y.; Kumano, T. *Macromolecules* **2004**, *37*, 4860.

(5) (a) LeBaron, P. C.; Wang, Z.; Pinnavaia, T. J. *Appl. Clay Sci.* **1999**, *15*, 11. (b) Ray, S. S.; Okamoto, M. *Prog. Polym. Sci.* **2003**, *28*, 1539. (c) Morgan, A. B. *Mater. Matters* **2007**, *2*, 20.

(6) Adame, D.; Beall, G. W. *Appl. Clay Sci.* **2009**, *42*, 545−552.

(7) Medalia, Al.; Krauss, G. Reinforcement of Elastomers by Particulate Fllers. In *Science and Technology of Rubber*, 2nd ed.; Mark, J. E., Erman, B., Erich, F. R., Eds.; Academic Press: San Diego, CA, USA, 1994; pp 387−418.

(8) Sternstein, S. S.; Zhu, A. J. *Macromolecules* **2002**, *35*, 7262.

(9) Lin, G.; Tian, M.; Lu, Y. L.; Zhang, X. J.; Zhang, L. Q. *Polymer* **2006**, *38*, 498−502.

(10) Yahaya1, L. E.; Adebowale, K. O.; Menon, A. R. R.; Rugmini, S.; Olu-Owolabi, B. I.; Chameswary, J. *Afr. J. Pure Appl. Chem.* **2010**, *4*, 198−205.

(11) Sui, G.; Zhong, W. H.; Yang, X. P.; Yu, Y. H. *Mater. Sci. Eng., A* **2008**, *485*, 524−531.

(12) González, J. C.; Retsos, H.; Verdejo, R.; Toki, S.; Hsiao, B. S.; Giannelis, E. P.; López-Manchado, M. A. *Macromolecules* **2008**, *41*, 6763−6772.

(13) Al-Hartomy, O. A.; Al-Ghamdi, A. A.; Al-Salamy, F.; Dishovsky, N.; Shtarkova, R.; Iliev, V.; El-Tantawy, F. *Int. J. Mater. Chem.* **2012**, *2*, 116−122.

(14) (a) Prud'homme, R. K.; Ozbas, B.; Aksay, I. A.; Register, R. A.; Adamson, D. H. W.O. Patent 2008045778 A1, 2008. (b) Kim, H.; Miura, Y.; Macosko, C. W. *Chem. Mater.* **2010**, *22*, 3441−3450.

(15) Kim, H.; Macosko, C. W. *Polymer* **2009**, *50*, 3797. Kim, H.; Macosko, C. W. *Macromolecules* **2008**, *41*, 3317−3327.

(16) Bindu, P.; Joseph, R.; Thomas, S. *Sci. Adv. Mater.* **2013**, *5*, 116−126.

(17) Visakh, P. M.; Thomas, S.; Oksman, K.; Mathew, A. P. *BioResources* **2012**, *7*, 2156−2168.

(18) Visakh, P. M.; Thomas, S.; Oksman, K.; Mathew, A. P. *Composites, Part A* **2012**, *43*, 735−741.

(19) (a) Hepburn, C. *Rubber Technol. Intern.* **1985**, *24*, 5. (b) Hepburn, C.; Mahdi, M. S. *Kautsch. Gummi Kunstst.* **1986**, *39*, 629. (c) Hepburn, C.; Mahdi, M. S. *Plast. Rubber Process. Appl.* **1986**, *6*, 247. (d) Hepburn, C.; Mahdi, M. S. *Plast. Rubber Process. Appl.* **1986**, *6*, 257. (e) Hepburn, C.; Mahdi, M. S. *Plast. Rubber Process. Appl.* **1986**, *6*, 267. (f) Hepburn, C.; Halim, M. H..; Mahdi, M. S. *Kautsch. Gummi Kunstst.* **1990**, *43*, 794.

(20) (a) Sahoo, N. G.; Das, C. K.; Pandaand, A. B.; Pramanik, P. *Macromol. Res.* **2002**, *10*, 369. (b) Yu, Y. *Tire Ind.* **2002**, *22*, 729. (c) Zhu, S. L.; Shiand, S. T.; Xu, J. W. *China Elastomerics* **2002**, *12*, 48.

(21) (a) Sahoo, S.; Maiti, M.; Ganguly, A.; George, J. J.; Bhowmick, A. K. *J. Appl. Polym. Sci.* **2007**, *105*, 2407. (b) Begum, P. M. S; Joseph, R.; Yusuff, K. K. M. *Prog. Rubber Plast. Recycl. Technol.* **2008**, *24*, 141. (c) Bindu, P.; Biji, N. M.; Thomas, S. Natural Rubber Nanocomposites: Role of nano ZnO in Natural Rubber. In *The Proceedings of the 2nd International Symposium on Advanced Materials and Polymers for Aerospace and Defence Applications: SAMPADA-2008*, Pune, India, Dec 8−12, 2008; Vora, R. H., Ed.; Elsevier: Amsterdam, 2008.

(22) Begum, P. M. S; Yusuff, K. K. M.; Joseph, R. *Int. J. Polym. Mater.* **2008**, *57*, 1083.

(23) Chapman, A.; Johnson, T. *Kautsch. Gummi Kunstst.* **2005**, *58*, 358.

(24) (a) Sharma, S. C. *Positron Annihilation Studies of Fluids*; World Science: Singapore, 1988; p 1431. (b) Jobando, V. O.; Quarles, C. A. *Phys. Status Solidi C* **2007**, *4*, 3763.

(25) Jean, Y. C. *Microchem. J.* **1990**, *42*, 72.

(26) (a) Yongshang, L.; Weng, L.; Zang, L. *Biomacromolecules* **2004**, *5*, 1046. (b) Sriupayo, J.; Supaphol, P.; Blackwell, J.; Rujiravanit, R. *Carbohydr. Polym.* **2005**, *62*, 130.

(27) Joseph, A.; Mathai, A. E.; Thomas, S. *J. Membr. Sci.* **2003**, *220*, 13.

(28) Stephen, R.; Varghese, S.; Joseph, K.; Oommen, Z.; Thomas, S. *Polymer* **2006**, *47*, 858.

(29) Ellis, B.; Welding, G. N. *Techniques of Polymer Science*; Society for Chemical Industry: London, 1964; p 46.

(30) Hildebrand, J. H.; Scott, R. I. *The Solubility of Non-Electrolytes*, 3rd ed.; Reinhold: New York, 1949.

(31) Usuki, A.; Kawasumi, M.; Kojima, Y.; Okada, A.; Kurauchi, T.; Kamigaito, O. *J. Mater. Res.* **1993**, *8*, 1174.

(32) Hagiwara, K.; Ougizawa, T.; Inoue, T.; Hirata, K.; Kobayashi, Y. *Radiat. Phys. Chem.* **2000**, *58*, 525.

(33) Pethrick, R. A. *Prog. Polym. Sci.* **1997**, *22*, 1.

(34) Berriot, J.; Lequeux, F.; Monnerie, L.; Montes, H.; Long, D.; Sotta, P. *J. Non-Cryst. Solids* **2002**, *307*, 719−724.

(35) Wang, Y. C.; Fan, S. C.; Lee, K. R.; Li, C. L.; Huang, S. H.; Tsai, H. A.; et al. *J. Membr. Sci.* **2004**, *239*, 219.

(36) Warrick, E. L.; Pierce, O. R.; Polmanteer, K. E.; Saam, J. C. *Rubber Chem. Technol.* **1979**, *52*, 437.

(37) Meera, A. P. Effect of Spherical and Layered Type Fillers on the Morphology and Physico-Mechanicl Properties of Natural Rubber Nanocomposites. Ph.D. Thesis, Mahatma Gandhi University, Kottayam, Kerala, India, 2010.

(38) Rotter, G.; Ishida, H. *Macromolecules* **1992**, *25*, 2170−2176.
(39) Tsagaropoulos, G.; Eisenberg, A. *Macromolecules* **1995**, *28*, 6067−6077.
(40) Mayes, A. M. *Nat. Mater.* **2005**, *4*, 651−652.
(41) Starr, F. W.; Schrøder, T. B.; Glotzer, S. C. *Phys. Rev. E* **2001**, *64*, 021802.
(42) Chua, P. S. *Polym. Compos.* **1986**, *8*, 308−313.
(43) Bliznakove, E. D.; White, C. C.; Shaw, M. T. *J. Appl. Polym. Sci.* **2000**, *77*, 3220−3227.
(44) (a) Dickie, R. A. *J. Polym. Sci., Polym. Phys. Ed.* **2003**, *14*, 2073−2082. (b) Liang, J. Z. *J. Thermoplast. Compos. Mater.* **2011**, *24*, 207−215.
(45) Abdalla, M.; Dean, D.; Adibempe, D.; Nyairo, E.; Robinson, P.; Thompson, G. *Polymer* **2007**, *48*, 5662−5670.
(46) Cowie, J. M. G. *Polymers: Chemistry and Physics of Modern Materials*, 2nd ed.; Nelson Thornes Ltd.: Cheltenham, U.K., 2000; pp 375−390.
(47) Nielsen, L. E.; Landel, R. F. *Mechanical Properties of Polymers and Composites*, 2nd ed.; Hanser Publishers: New York, 1992; pp 45−67, 495.
(48) Mc Nally, T.; Pötschke, P.; Halley, P.; Murphy, M.; Martin, D.; Bein, D.; Bell, S.; Brennan, G.; Lemoine, P. *Polymer* **2005**, *46*, 8222−8232.
(49) Nielsen, L. E.; Landel, R. F. *Mechanical Properties of Polymers and Composites*, 2nd ed.; Marcel Dekker: New York, 1994; pp 141−142, 436−437.
(50) (a) Kojima, Y.; Usuki, A.; Kawasumi, M.; Okada, A.; Kurauchi, T.; Kamigaito, O. *J. Appl. Polym. Sci.* **1993**, *49*, 1259−1264. (b) Kojima, Y.; Usuki, A.; Kawasumi, M.; Okada, A.; Fukushima, Y.; Kurauchi, T.; Kamigaito, O. *J. Mater. Res.* **1993**, *8*, 1185−1189.
(51) Shelley, J. S.; Mather, P. T.; DeVries, K. L. *Polymer* **2001**, *42*, 5849−5858.
(52) Wilkinson, A. N.; Man, Z.; Stanford, J. L.; Matikainen, P.; Clemens, M. L.; Lees, G. C.; Liauw, C. M. *Macromol. Mater. Eng.* **2006**, *291*, 917−928.
(53) Rao, Y. Q.; Pochan, J. M. *Macromolecules* **2007**, *40*, 290−296.
(54) (a) Simha, R.; Utracki, L. A.; Garcia-Rejon, A. *Compos. Interfaces* **2001**, *8*, 345−353. (b) Simha, R.; Utracki, L. A.; Garcia-Rejon, A. *Macromolecules* **2003**, *36*, 2114−2121. (c) Tanoue, S.; Utracki, L. A.; Garcia-Rejon, A.; Tatibouet, J.; Cole, K. C.; Kamal, M. R. *Polym. Eng. Sci.* **2004**, *44*, 1046−1060.
(55) Zhang, X.; Loo, L. S. *Macromolecules* **2009**, *42*, 5196−5207.
(56) Miltner, H. E.; Assche, G. V.; Pozsgay, A.; Pukaszky, B.; Mele, B. V. *Polymer* **2006**, *47*, 826−835.
(57) Burnside, S. D.; Giannelis, E. P. *J. Polym. Sci., Part B: Polym. Phys.* **2000**, *38*, 1595−1604.
(58) Luo, H.; Kluppel, M.; Schneider, H. *Macromolecules* **2004**, *37*, 8000.
(59) (a) Litvinov, V. M.; Steeman, P. A. M. *Macromolecules* **1999**, *32*, 8476. (b) Leu, G.; Liu, Y.; Werstler, D. D.; Cory, D. G. *Macromolecules* **2004**, *37*, 6883.
(60) (a) Wang, M. J. *Rubber Chem. Technol.* **1998**, *71*, 520. (b) Berriot, J.; Montes, H.; Lequeux, F.; Long, D.; Sotta, P. *Macromolecules* **2002**, *35*, 9756. (c) Montes, H.; Lequeux, F.; Berriot, J. *Macromolecules* **2003**, *36*, 8107. (d) Merabia, S.; Sotta, P.; Long, D. R. *Macromolecules* **2008**, *41*, 8252.
(61) Heinrich, G.; Kluppel, M. Recent Advances in the Theory of Filler Networking in Elastomers. In *Filled Elastomers Drug Delivery Systems*; Arora, M.; et al., Eds.; Advances in Polymer Science; Springer: Berlin, 2002; Vol. *160*.
(62) Song, M.; Xia, H. S.; Yao, K. J.; Hourston, D. J. *Eur. Polym. J.* **2005**, *41*, 259.
(63) Kohjiya, S.; Kato, A.; Ikeda, Y. *Prog. Polym. Sci.* **2008**, *33*, 979.
(64) Hong, J. I.; Schadler, L. S.; Siegel, R. W.; Mårtensson, E. *Appl. Phys. Lett.* **2003**, *82*, 1956−1958.
(65) (a) Wu, S. *Polymer* **1985**, *26*, 1855;(b) *J. Appl. Polym. Sci.* **1988**, *35*, 549.
(66) Wang, Z.; Liu, J.; Wu, S.; Wang, W.; Zhang, L. *Phys. Chem. Chem. Phys.* **2010**, *12*, 3014−3030.
(67) Nelson, J. K.; Hu, Y. The Impact of Nanocomposite Formulations on Electrical Voltage Endurance. In *Proceedings of the IEEE International Conference of Solid Dielectrics, 2007: ICSD'07*, Winchester, U.K., 5−9 July 2004; Vol. *2*, pp 832−835.